A clock in mouse cones contributes to the retinal oscillator network and to synchronization of the circadian system

Cristina Sandu[1*#], Prapimpun Wongchitrat[2*], Nadia Mazzaro[1], Catherine Jaeger[1], Hugo Calligaro[1], Jorge Mendoza[1], David Hicks[1], Marie-Paule Felder-Schmittbuhl[1#]

[1] Centre National de la Recherche Scientifique, Université de Strasbourg, Institut des Neurosciences Cellulaires et Intégratives, 67000 Strasbourg, France

[2] Center for Research and Innovation, Faculty of Medical Technology, Mahidol University, 73170 Salaya, Nakon Pathom, Thailand

[*] Equal contribution

[#] **Corresponding authors :** feldermp@inci-cnrs.unistra.fr; sandu@inci-cnrs.unistra.fr

Key Words: Nrl, cone, circadian rhythm, phase resetting, retinal clock, negative masking

Abbreviations: Cnga3, Cyclic Nucleotide Gated Channel Subunit Alpha 3; Crx**,** Cone-Rod Homeobox.

Abstract

Multiple circadian clocks dynamically regulate mammalian physiology. In retina, rhythmic gene expression serves to align vision and tissue homeostasis with daily light changes. Photic input is relayed to the suprachiasmatic nucleus to entrain the master clock, which matches behaviour to environmental changes. Circadian organization of the mouse retina involves coordinated, layer-specific oscillators, but so far little is known about the cone photoreceptor clock and its role in the circadian system. Using the cone-only *Nrl*$^{-/-}$ mouse model we show that cones contain a functional self-sustained molecular clockwork. By bioluminescence-combined imaging we also show that cones provide substantial input to the retinal clock network. Furthermore, we found that light entrainment and negative masking in cone-only mice are subtly altered and that constant light displayed profound effects on their central clock. Thus, our study demonstrates the contribution of cones to retinal circadian organisation and their role in finely tuning behaviour to environmental conditions.

Introduction

Adaptation of behaviour and physiology to the 24 h light/dark (LD) cycle produced by the Earth's rotation around its axis is one of the main constraints affecting living organisms. Such adaptation is mediated by the circadian system, a network of tissue/cell-specific oscillators with an internal period close to (circa) 24 h, which in mammals is coordinated by a master clock located in the hypothalamic suprachiasmatic nuclei (SCN) (for review: (Hastings, Maywood, & Brancaccio, 2019)). Daily behavioural and physiological rhythms are controlled by cell autonomous molecular oscillators constituted of oscillating auto-regulatory clock transcription factors able to drive gene expression programs, hence cellular physiology. The retina plays a particular role in the circadian system in mammals because it is responsible for the unique photosensory input to ensure entrainment of the clock in the SCN to the LD cycle (Yamazaki, Goto, & Menaker, 1999).

The retina was the first circadian clock identified outside the SCN, based on the capacity of explanted tissue from hamsters to secrete melatonin in a rhythmic manner (Tosini & Menaker, 1996). Since the retinal clock is able to synchronize to the LD cycle *in vitro*, this tissue constitutes on its own a complete circadian system, with molecular clock machinery, resetting input mechanism and biological outputs (Felder-Schmittbuhl et al., 2018; McMahon, Iuvone, & Tosini, 2014). Besides melatonin synthesis the retina displays a plethora of rhythmic properties, including expression of photopigment genes, processing of light information, phagocytosis of photoreceptor outer segments, metabolism, together contributing to adapt visual function to the LD cycle and ensuring tissue homeostasis (for review (Felder-Schmittbuhl, Calligaro, & Dkhissi-Benyahya, 2017)). Given the complexity of the retinal tissue comprising glial cells and six major types of neurons, identification of the cell type(s) constituting its main oscillator has been a matter of debate. Analysis of clock gene expression

in vitro and *ex vivo* suggested that the retina is composed of several layer-specific, coupled oscillators (Dkhissi-Benyahya et al., 2013; Jaeger et al., 2015; Sandu, Hicks, & Felder-Schmittbuhl, 2011) but the existence/identity of a main driver remains under question. Several lines of evidence, notably the presence of melatonin synthesis machinery (Gianesini, Clesse, Tosini, Hicks, & Laurent, 2015; Niki et al., 1998), the detection of cycling clock factors (Liu, Zhang, & Ribelayga, 2012), have pointed to cones as a potential retinal clock component but their precise contribution to the network has not been evaluated.

The retina possesses a laminar organisation as well as parallel microcircuits processing light information. Photon capture occurs in photoreceptors, highly specialized cells located in the outer retina. Cones respond to bright light (photopic vision) and mediate color vision whereas rods are much more sensitive and function under low intensities (scotopic vision). In mice, most cones (95%) are M-cones which express 2 types of opsins (short wavelength - sws, with maximal sensitivity at 360 nm and middle wavelength – mws, with peak sensitivity at 509 nm) and a minority of these cones express either the blue or the green opsin alone respectively in the ventral and dorsal regions of the retina (Applebury et al., 2000; Hughes, Watson, Foster, Peirson, & Hankins, 2013). Investigation of cone properties has been challenging given their low number in retinas of routinely used laboratory mammals, i.e., <3% of total photoreceptors in mice (Jeon, Strettoi, & Masland, 1998) and <1% in rats (Szel & Rohlich, 1992). The *Nrl*$^{-/-}$ mouse (Mears et al., 2001), in which absence of the NRL transcription factor totally blunts rod generation, has a cone-only retina with a majority of S-cones, and has been extensively used to study cone properties without the interference from rods (Krigel, Felder-Schmittbuhl, & Hicks, 2010; Liu et al., 2012; Wenzel et al., 2007).

Studies from the last 20 years have led to improved understanding of how information linked to light perception in the eye is conveyed to the SCN and translated into a message reflecting

the alternation of day and night, able to entrain the central clock. In particular, a minor, light-sensitive population of retinal ganglion cells (RGC) expressing the melanopsin photopigment (intrinsically photosensitive RGC or ipRGC) constitutes the (unique) cellular connection between the retina and the SCN (Goz et al., 2008; Guler et al., 2008; Hatori et al., 2008). Despite the major role played by these blue sensors (peak sensitivity = 480 nm), some data demonstrate a role for rods in synchronisation to the LD cycle at low light intensities (Altimus et al., 2010; Boudard, Mendoza, & Hicks, 2009; Lall et al., 2010) and also for cones (Dkhissi-Benyahya, Gronfier, De Vanssay, Flamant, & Cooper, 2007; van Diepen, Ramkisoensing, Peirson, Foster, & Meijer, 2013; van Oosterhout et al., 2012). In addition, recent results in mice suggested that cones also play a role in entrainment mechanisms by perceiving spectral changes characteristic of dusk or dawn (Mouland, Martial, Watson, Lucas, & Brown, 2019; Walmsley et al., 2015). However, these functions have not been investigated with gain of function mutants, in particular for cones.

Here we investigate the role of murine cones in the circadian system. We show that cones in the *Nrl*$^{-/-}$ retina harbor a functional molecular clock, the elements of which are similar to other central or peripheral clocks. Furthermore, the cone population contributes, together with the inner and ganglion cell layers, to the oscillatory network of the retina. However, light-mediated behavior seems to be altered in the cone-only retina from *Nrl* mutant mice in acute and chronic light exposure conditions, particularly at low light intensities. This suggests that total replacement of rods by cones induces modifications in the global non-image forming visual function of the retina in mice.

Results

A functional clock in cone photoreceptors

We first aimed to characterize the cone molecular clock on microdissected photoreceptors isolated from the *Nrl* KO mice over 24 h in DD (Figure 1A). We found that all core clock gene transcripts examined, *Bmal1, Clock, Per1, Per2, Per3, Cry1, Cry2, Rev-Erbα, Rorβ* are expressed in cones (Figure 1B, top panel). Significant rhythmic levels of expression were determined for *Bmal1, Per1, Per2, Per3, Rev-Erbα* (Table 1). Interestingly, the expression profile of *Bmal1* was in opposite phase in comparison to the profiles of *Per* transcripts, as described in the SCN (King & Takahashi, 2000; Welsh, Takahashi, & Kay, 2010) and other peripheral tissues such as liver (Noguchi et al., 2010; Oishi, Sakamoto, Okada, Nagase, & Ishida, 1998). 24 h profiles in cones were also similar, at least for *Bmal1* and *Per1* transcripts, to those reported for mouse whole retinas sampled in DD (Ruan, Allen, Yamazaki, & McMahon, 2008).

We also investigated the expression of several well-known or putative target genes of the retinal clock such as *S-opsin, M-opsin, Crx, arrestin 3, Cnga3* and *c-Fos* transcripts (Figure1 B, lower panel). *S-opsin, arrestin 3* and *Cnga3*, expressed in S-cones (Mears et al., 2001), displayed significantly rhythmic profiles (Table 1).

To further evaluate the capacity of cones to sustain rhythmicity, we used a vibratome-based sectioning of the retina to isolate photoreceptor (cone-only) layers from the KO mice raised on the $Per2^{Luc}$ reporter background (Yoo et al., 2004) for real-time bioluminescence recordings. Photoreceptor layers from WT mice were used as control. As previously described (Jaeger et al., 2015) the latter showed robust PER2:: LUC oscillations with a 26.46 ± 0.02 h period (Figure 1C). Cone layers from the KO retinas also proved robustly rhythmic in culture, but yet with a significantly longer period: 29.07 ± 0.03 h (n = 6 for WT, n = 9 for KO; genotype effect: $p = 0.018$) (Figure 1C).

Finally, we examined how cone layers oscillate within the context of the whole retina by using in vitro real-time bioluminescence combined with imaging. 100 µm transversal sections were cut using the vibratome technique illustrated in Figure 1D, transferred on a semipermeable membrane, then cultured and imaged for several days in a temperature controlled microscope chamber. PER2 bioluminescence signal emerged from all layers, with higher intensity in ganglion and inner cell layers and weaker signal in the outer, photoreceptor layer (Figure 1E). Moreover, the PER2 signal was rhythmic in all layers (Figure 1F), with distinct free-run periods (24.28 ± 0.26 h for ganglion cell layers, 27.79 ± 0.20 h for inner nuclear layers and 26.80 ± 1.19 h for photoreceptor layers; Figure 1G) (significant layer effect, $p = 0.037$). Taken together, these data confirm the presence of an autonomous clock in cones.

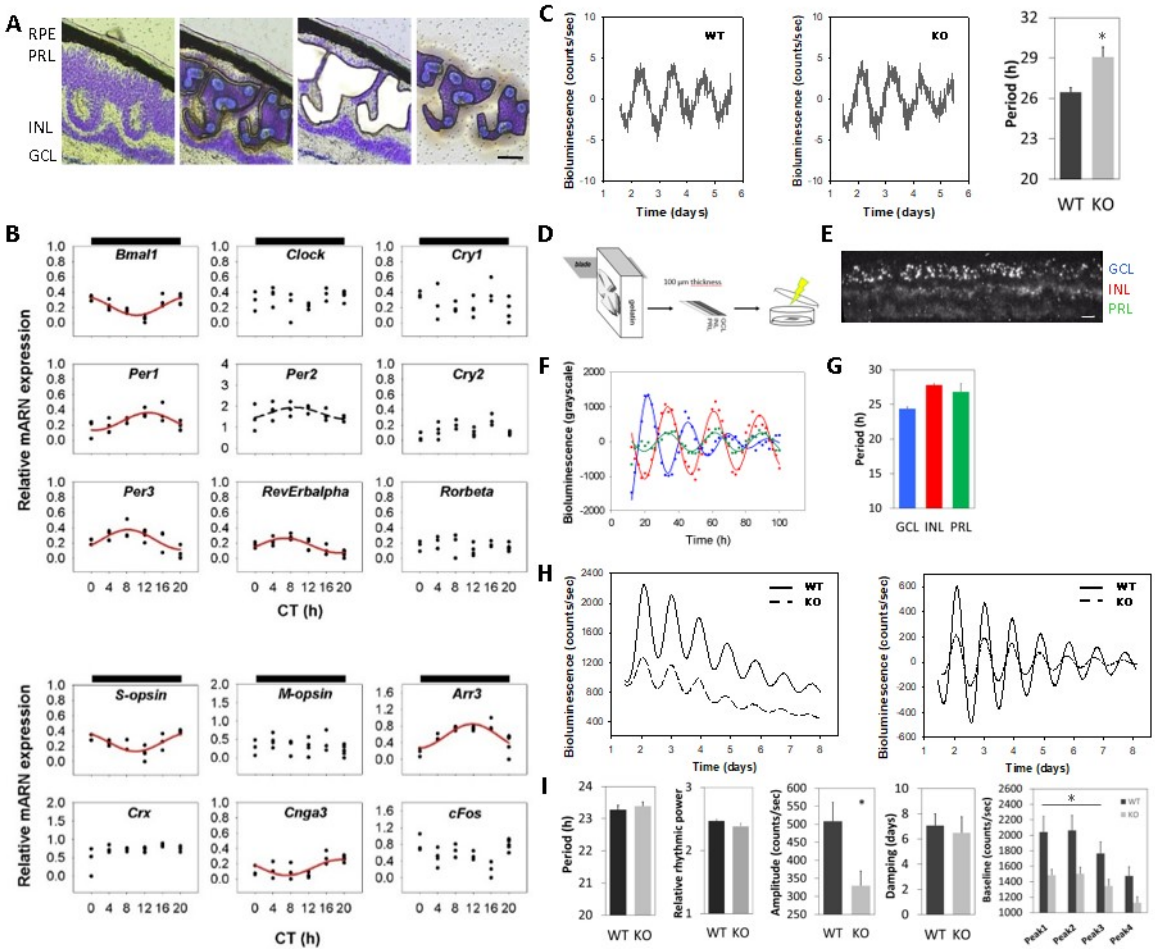

Figure 1: Circadian rhythms in cones and cone-only retinas

(A-C) A functional clock in cone photoreceptors. (A) Cone photoreceptors were microdissected from retinas of *Nrl*$^{-/-}$ mice sampled throughout 24 h in constant dark. The successive pictures show, from left to right: the characteristic structure of a cresyl-violet stained retinal section from these 1.5 month *Nrl*$^{-/-}$ mice with numerous rosettes; the capture/sectioning strategy; the same section after laser cut; the resulting captured sample. The distinct retinal layers (GCL, ganglion cell layer; INL, inner nuclear layer; PRL, photoreceptor layer) and the retinal pigmented epithelium (RPE) are indicated (scale bar = 50 µm). (B) Circadian expression profiles of clock genes (top) and clock output genes (bottom) in microdissected cone layers sampled every 4 h in DD (CT = Circadian Time, corresponding to projected ZT). Expression was analysed by qRT-PCR (data for each sample are presented as relative expression level with respect to a WT photoreceptor calibrator: n = 3-5 per time point). Traces represent the best-fitted sinusoidal regressions supporting rhythmic gene expression in the cases where both cosinor analysis and ANOVA yielded significant *p* values. Dashed lines when only cosinor proved significant. Results from statistical analyses are shown in Table 1 and Figure1- figure supplement 1. (C) PER2::LUC rhythms in explanted

cone layers. Graphs show representative (baseline-subtracted) bioluminescence recordings of photoreceptor layers isolated by vibratome sectioning from WT (left) and KO (right) mice. Periods of oscillations proved significantly longer in mutants (n = 6 for WT, n = 9 for KO; t-test, $p = 0.018$). (D-G) Bioluminescence imaging of retinal transversal section from *Nrl*$^{-/-}$ mice reveals sustained oscillation capacity in cones. (D) Schematic presentation of the vibratome-based strategy for isolating a transversal 100 µm thick section from a freshly dissected retina. (E) Representative picture showing bioluminescence emission in the 3 neuronal layers from a *Nrl*$^{-/-}$ section (exposure time = 2 h, scale bar = 100 µm). (F) Representative bioluminescence counts from the 3 neuronal layers taken individually in one *Nrl*$^{-/-}$ sample. Damped sinusoids represent the best-fit to subtracted data. (G) Periods were calculated separately for each cell layer and show a significant layer effect (n = 3, $p = 0.037$). (H,I) Circadian rhythms are altered in a cone-only retina. (H) Representative raw (left) and baseline-subtracted (right) bioluminescence recordings from WT (solid line) and KO (dashed line) whole retinas showing reduced baseline and amplitude of the cone-only, mutant retinas. (I) Period, relative rhythmic power, amplitude, damping and baseline levels were compared between WT and mutant retinas and revealed a significant difference in amplitude (t-test, $p = 0.013$) and baseline levels (repeated measures 2-way ANOVA, $p = 0.015$) between genotypes (n = 12 per genotype). Results are represented as mean ± SEM. *: $p < 0.05$.

Figure 1-Source Data 1: Raw data of results shown in Figure 1

Figure 1-figure supplement 1: Power calculation for cosinor test and ANOVA of gene expression results

Figure 1-figure supplement 2: No major change in retinal cell types besides photoreceptors in *Nrl*$^{-/-}$ mice

168

Gene	$p_{cosinor}$	$F_{cosinor}$	**a**	p_a	**b**	p_b	**c**	p_c	p_{ANOVA}	F_{ANOVA}
Bmal1	<0.0001	F(2, 19) = 19.29	0.221	<0.0001	0.123	<0.0001	22.13	<0.0001	<0.001	F(5, 21) = 12.89
Clock	0.1851	F(2, 19) = 1.84	0.303	<0.0001	0.062	0.07	21.58	<0.0001	0.21	F(5, 21) = 1.63
Cry1	0.9489	F(2, 19) = 0.05	0.248	<0.0001	0.015	0.74	21.82	0.0866	0.12	F(5, 21) = 2.08
Cry2	0.1435	F(2, 19) = 2.15	0.132	<0.0001	0.054	0.05	12.38	<0.0001	0.006	F(5, 21) = 5.09
*Per1**	0.0014	F(2, 19) = 9.75	0.245	<0.0001	0.115	0.0003	12.81	<0.0001	0.02	F(5, 20) = 12.90
*Per2**	0.0326	F(2, 19) = 4.17	1.653	<0.0001	0.286	0.0098	8.99	<0.0001	0.22	Eqvar failed
*Per3**	0.001	F(2, 19) = 10.41	0.245	<0.0001	0.13	0.0002	8.25	<0.0001	0.007	F(5, 20) = 4.94
Rev-Erbα	<0.0001	F(2, 19) = 17.56	0.168	<0.0001	0.096	<0.0001	6.72	<0.0001	0.001	F(5, 21) = 7.22
Rorβ	0.6356	F(2, 19) = 0.46	0.161	<0.0001	0.023	0.34	2.94	0.45	0.71	F(5, 21) = 0.585
M-opsin	0.6325	F(2, 19) = 0.47	0.324	<0.0001	0.06	0.34	7.09	0.09	0.49	F(5, 21) = 0.489
S-opsin	<0.0001	F(2, 19) = 16.47	0.252	<0.0001	0.12	<0.001	21.94	<0.0001	<0.0001	F(5, 21) = 9.08
Arrestin 3	<0.0001	F(2, 19) = 17.89	0.56	<0.0001	0.288	<0.0001	11.7	<0.0001	0.004	Norm failed
Cnga3	0.003	F(2, 19) = 8.04	0.15	<0.0001	0.103	0.0008	19.1	<0.0001	0.001	F(5, 21) = 7.168
Crx	0.1929	F(2, 19) = 1.80	0.698	<0.0001	0.099	0.07	13.35	<0.0001	0.11	Norm failed
c-Fos	0.0809	F(2, 19) = 2.88	0.581	<0.0001	0.169	0.03	0.06	0.9689	0.002	F(5, 21) = 6.635

169

170 **Table 1: Cosinor analysis and ANOVA for gene expression results**

171 (a, mesor; b, amplitude; c, acrophase)

172 * One outlier sample was removed from analysis

173

174

Gene	cosinor	ANOVA
	Power (alpha = 0.05)	Power (alpha = 0.05)
Bmal1	**1**	**0.999**
Clock	0.175	0.314
Cry1	0.282	0.046
Cry2	**0.86**	0.518
*Per1**	0.675	**0.971**
*Per2**	0.138	0.771
*Per3**	**0.834**	**0.977**
Rev-Erbα	**0.973**	**0.998**
Rorβ	0.05	0.158
M-opsin	0.05	0.159
S-opsin	**0.995**	**0.954**
Arrestin 3	**0.998**	**0.998**
Cnga3	**0.972**	**0.948**
Crx	0.422	0.452
c-Fos	**0.956**	0.63

175

176 **Figure 1-figure supplement 1: Power calculation for cosinor test and ANOVA of gene**
177 **expression results**

178 Power values > 0.8 are in bold.

179

Clock properties in a cone-only retina

We then examined how the unique presence of cones affects the overall circadian function in the mouse retina. Previous bioluminescence studies demonstrated that mouse retina displays oscillatory expression of PER2 (Jaeger et al., 2015; Ruan et al., 2008). To evaluate how a cone-only photoreceptor population impacts on the retinal clock we performed real-time bioluminescence recordings of whole retinal explants from *Nrl*$^{-/-}$ *Per2*^{Luc} mice, compared to WT controls (Figure 1H). Sustained circadian oscillations of PER2 bioluminescence were observed for several days, with no difference in period ($p = 0.557$), relative rhythmic power ($p = 0.273$) and damping ($p = 0.583$) comparing to the wild-type littermates (Figure 1I). However, the amplitude of the oscillations was significantly reduced in the mutants by 35% ($p = 0.013$). Moreover, a significant reduction of the baseline levels was observed in mutant mice as compared to wild-type ($p = 0.015$) (Figure 1H and 1I).

To make sure the observed effects were not induced by alterations of other cell types known to play a role in the retinal clock network, we evaluated whether the *Nrl*$^{-/-}$ mutation affected two retinal cell populations; the intrinsically photosensitive ganglion cells (ipRGC) which express melanopsin (OPN4) photopigment and the dopaminergic amacrine cells which express tyrosine hydroxylase (TH). Both total numbers of cells analyzed by immunostaining ($p = 0.433$ and $p = 0.176$, for OPN4 and TH respectively; Figure 1-figure supplement 2A,B) and mRNA levels quantified by real-time qRT-PCR of whole retinas ($p = 0.426$ and $p = 0.156$, respectively; Figure 1-figure supplement 2C) showed no significant differences between wild-type and mutant retinas. By contrast, we observed a 2-fold increase in the level of expression of *Opn1mw* in the *Nrl* mutants ($p < 0.0001$), as previously described (Calligaro et al., 2019; Mears et al., 2001). Despite normal number and phenotype of dopaminergic cells, KO retinas displayed altered dopamine metabolism in response to light (Figure 1-figure supplement 2D), as known for rodless retinas (Nir & Iuvone, 1994). Thus the changes related

206 to rhythms measured in vitro in the *Nrl*$^{-/-}$ retinas are likely to result mainly from their specific

207 photoreceptor composition.

208

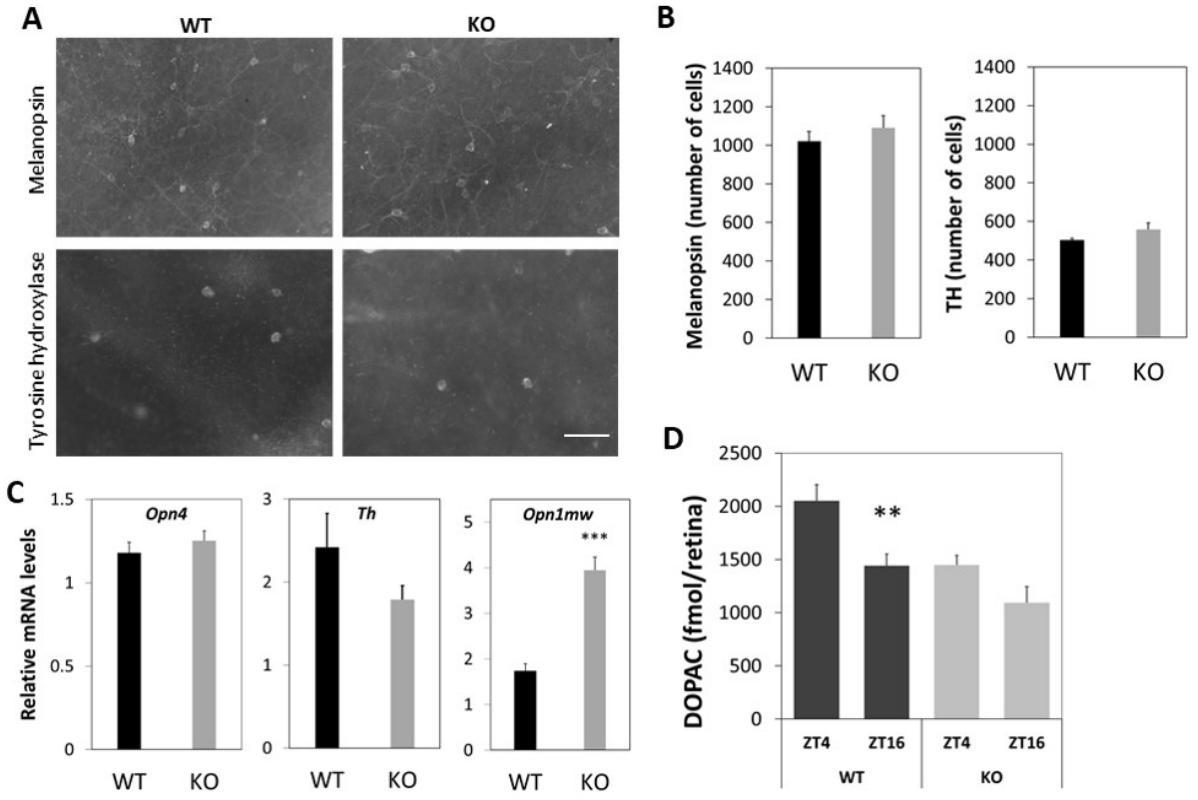

Figure 1-figure supplement 2: no major change in retinal cell types besides photoreceptors in *Nrl*$^{-/-}$ mice

(A) Immunolabelling of melanopsin (top) and TH (bottom) in whole-mount retinas of the WT and KO mice. (B) Quantification of melanopsin (left) and TH (right) positive cells in whole-mount retina. There is no significant difference between control and KO mice (WT n = 5, KO n = 6; $p > 0.05$). (C) Expression of *Opn4*, *Th* and *Opn1mw* transcripts in whole retina. The *Opn4* and *Th* levels do not change in the cone-only retinas ($p > 0.05$). The level of *Opn1mw* increased significantly comparing to WT retinas ($p < 0.0001$) (WT n = 7, KO n = 8). (D) Diurnal levels of DOPAC in *Nrl* KO mice are no longer rhythmic. DOPAC levels in whole retinas (n = 6 per group) were measured at ZT4 (day-time) and ZT16 (night-time) and are affected by genotype and time (2-way ANOVA, $p = 0.001$ for both). Higher levels of DOPAC were measured at ZT4 with respect to ZT16 in the wild-type animals but not in *Nrl* mutants (2-way ANOVA post hoc analysis: $p = 0.003$ and $p = 0.07$, respectively) indicating that the response to light is altered in the KO retinas, as previously described for rodless mice. Results are represented as mean ± SEM. **: $p < 0.01$. ***: $p < 0.0001$.

SCN-driven rhythms are preserved in the cone-only mouse

SCN explants from *Nrl*$^{-/-}$ *Per2*^{Luc} mice produced autonomous and sustained PER2::LUC oscillations for at least 6 days *in vitro* similar to those from WT (Figure 2A). The robustness of rhythms was similar between genotypes, based on the relative rhythmic power (p = 0.344), indicating that in the cone-only mutant the master clock is not impaired (Figure 2B). Moreover, there was no effect on the phase of the oscillations (p = 0.938) and on the amplitude (p = 0.476), period (p = 0.944) and damping (p = 0.09) (Figure 2C-F). Thus, the SCN clock is not affected by the absence of rods in the standard conditions in which it was evaluated here.

We also recorded wheel-running activity of the *Nrl*$^{-/-}$ *Per2*^{Luc} mice in order to determine their circadian phenotype. These behavioral studies were conducted under classical white spectrum light, to which KO mice respond similarly to WT (Figure 2-figure supplement 1). Activity profiles (Figure 2G, Figure 2-figure supplement 2) showed no significant differences between *Nrl* mutants and their wild-type littermates, in LD 12:12, regarding the amount of total activity (13459 ± 4542 counts/24 h vs 15653 ± 3544 counts/24 h in WT and KO mice respectively; p = 0.809), the *rho*-phase activity (785 ± 182 counts/24 h vs 315 ± 151 counts/24 h; p = 0.803) and *alpha*-phase activity (13221 ± 4566 counts/24 h vs 15338 ± 3583 counts/24 h; p = 0.748) levels (Figure 2H). The endogenous period was measured under free-run conditions in DD and showed similar values between WT (23.96 ± 0.10 h) and KO (23.85 ± 0.05 h) (p = 0.278) (Figure 2I).

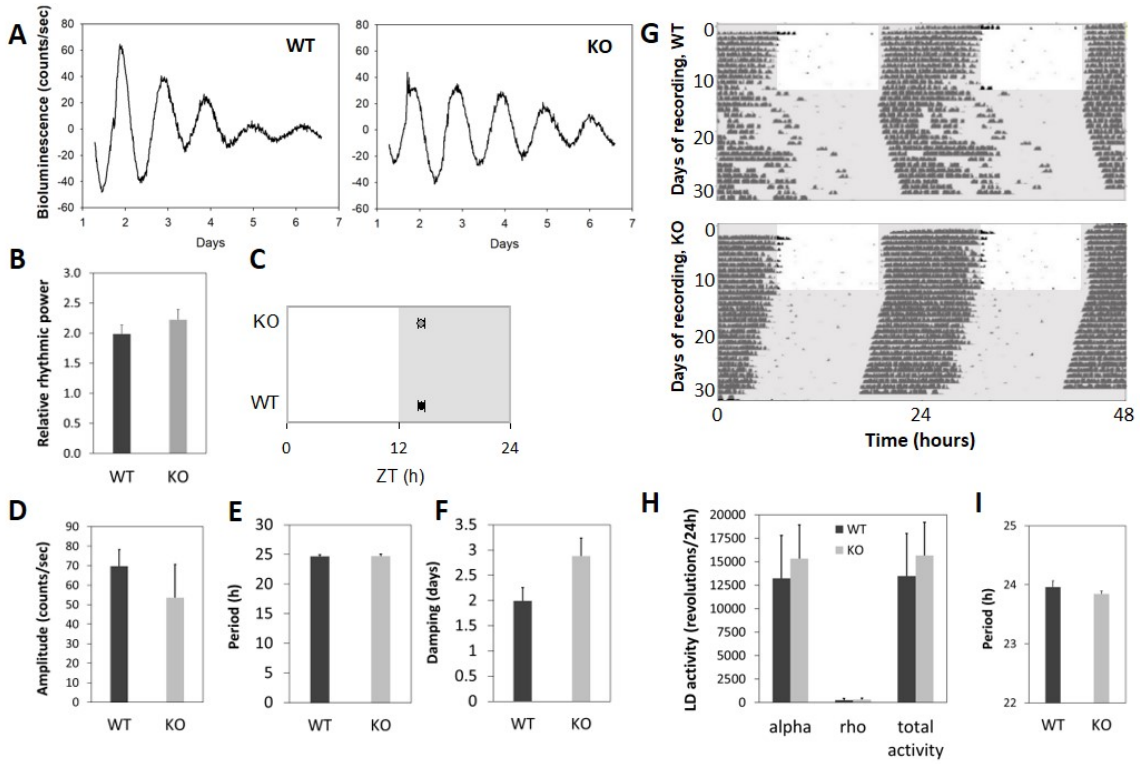

Figure 2: The cone-only retina does not affect the endogenous master clockwork

(A-F) The SCN oscillating capacity is not altered in the *Nrl*$^{-/-}$ mutant. (A) Representative PER2::LUC bioluminescence recordings (detrended data) of SCN explants from WT and *Nrl*$^{-/-}$ animals. No genotype effect was observed in the relative rhythmic power (B), phase of first peak (C; expressed relative to the LD cycle to which animals were previously exposed), amplitude (D), period (E) and damping (F) (n = 5 for WT, n = 7 for KO). (G-I) Actimetry recordings (wheel running) of WT and *Nrl*$^{-/-}$ mice show no genotype effect in both LD and DD conditions. (G) Representative actograms of WT (top) and KO (bottom) mice in 12h/12h LD cycle followed by constant darkness for 20 days. Grey shading indicates darkness. (H) Quantification of activity during the night-time (alpha), day-time (rho) and total 24 h in LD recordings, and of the endogenous periods measured in DD (I) showed no difference between genotypes (n = 4 for WT, n = 7 for KO). Results are represented as mean ± SEM.

Figure 2-Source Data 1: Raw data of experiments shown in figure 2

Figure 2-figure supplement 1: Light-adapted ERG responses in *Nrl*$^{-/-}$ mice are similar to WT.

Figure 2-figure supplement 2: Additional actograms of WT and KO mice in LD and DD condition

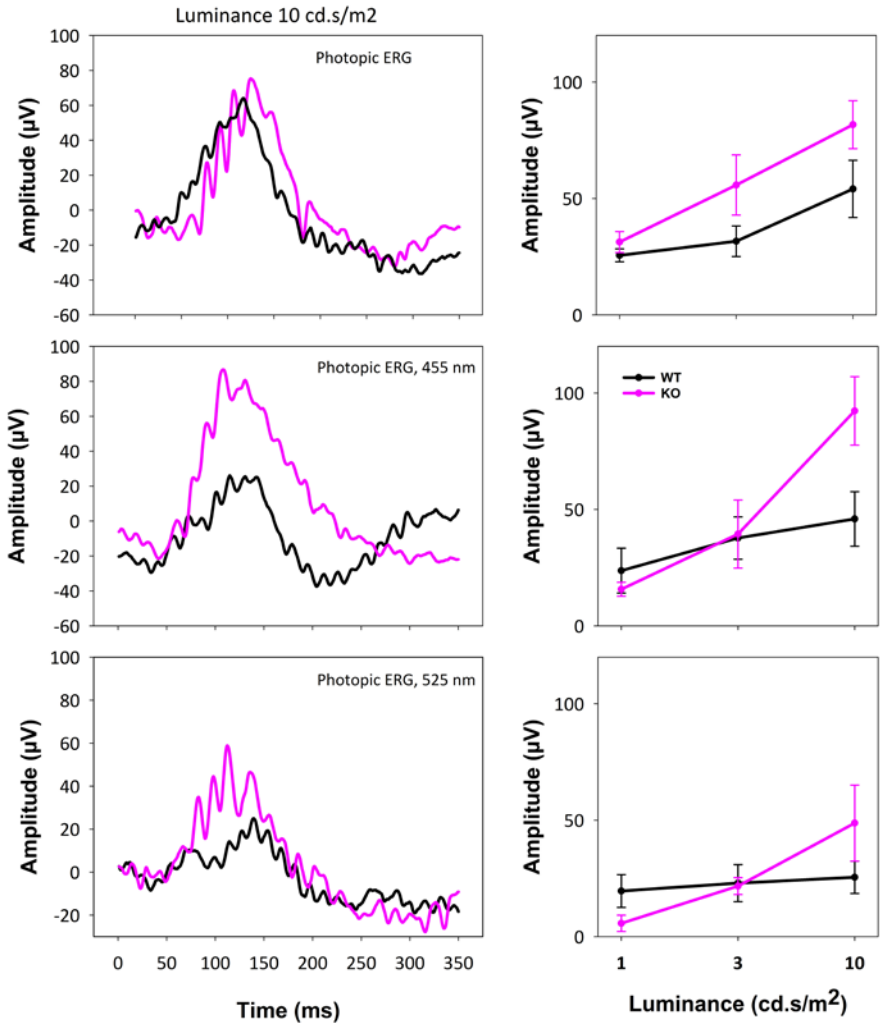

Figure 2-figure supplement 1: Light-adapted ERG responses in *Nrl*$^{-/-}$ mice are similar to WT.

(A) Representative waveforms of light-adapted ERG responses in photopic condition: white light (top) and two specific wavelengths - 455 nm (blue; middle) and 525 nm (green; bottom) - recorded at 10 cd.s/m^2 luminance in 6 week-old KO and WT mice. (B) Response-luminance curves of light-adapted WT and KO mice to stimuli of 1, 3 and 10 cd.s/m^2 (representative of cone function) in photopic condition (top) and at two wavelengths: 455 nm (middle) and 525 nm (bottom). The amplitude of b-waves is shown. In all cases two-way repeated measures ANOVA shows an effect of luminance. There is no genotype effect (n=5 for WT, n=3 for KO), suggesting comparable responses in WT and KO. However, there is a significant interaction between luminance and genotype for 455 nm (p = 0.015), with an increased response in KO mice at 10 cd.s/m^2 (post hoc analysis; p = 0.014). These results confirm that KO cones respond to light in the broad white spectrum light to which animals were exposed in our behavioral studies.

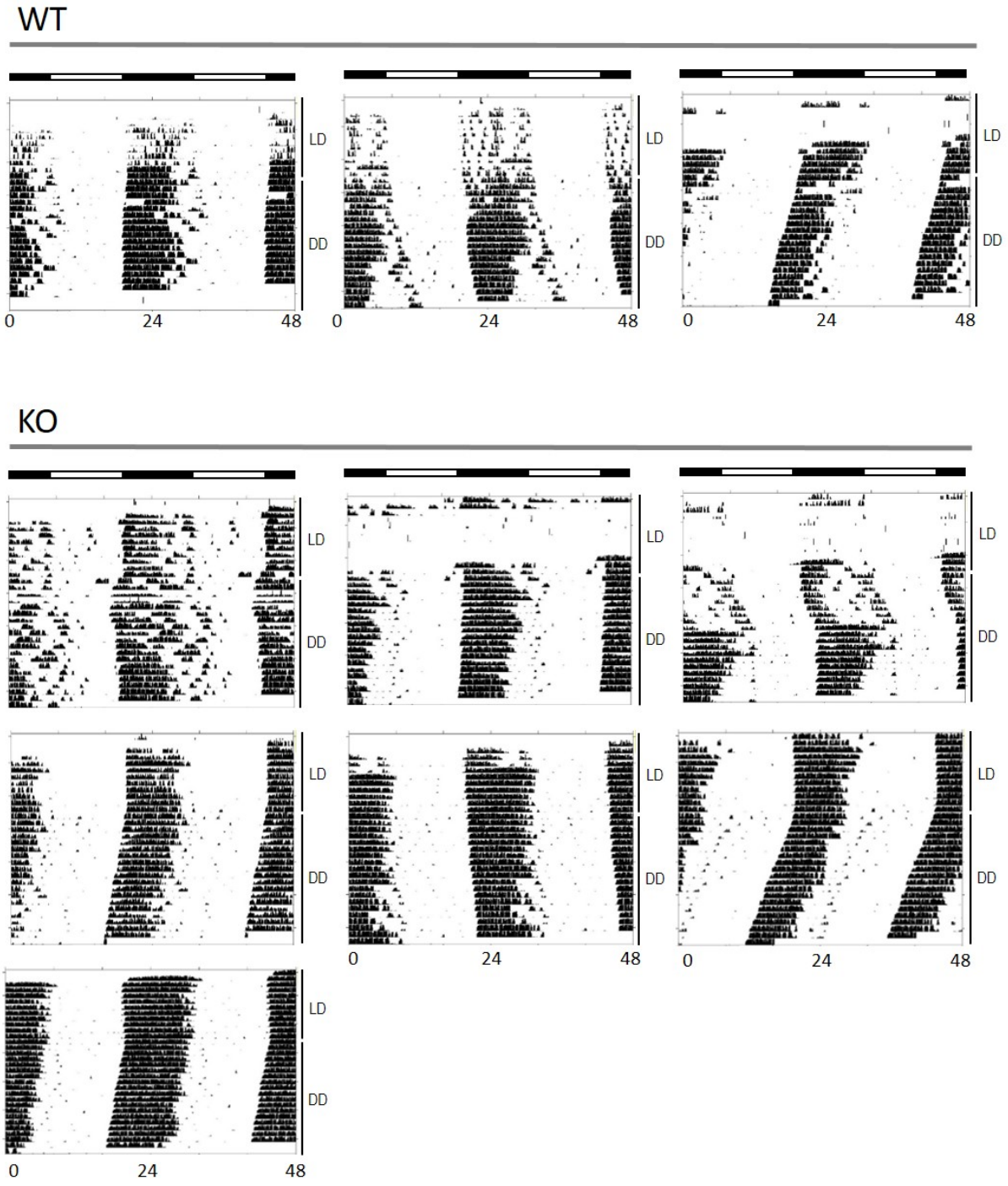

Figure 2-figure supplement 2: Additional actograms of WT and KO mice in LD and DD condition

Wheel-running activity of additional WT and KO mice also used for the analyses presented in Figure 2H,I. Note that in a few cases some LD data are missing due to technical recording problems.

Mild effects of acute light exposure

To evaluate behavioral response to acute light exposure, WT and KO mice were first exposed to a phase-resetting protocol. Thus, animals received a 15 min light pulse with different intensities, at the beginning of the constant dark period. Light pulses of high (170-220 lux), medium (14-20 lux) or low (1.0-1.3 lux) intensities provided at projected ZT15 induced a phase-delay in the onset of activity of both WT and *Nrl* mutant mice (Figure 3A). The ANOVA shows a light intensity effect on phase-shifts (2-way ANOVA, $p = 0.006$), but not a genotype effect ($p = 0.251$) nor an interaction between light intensity and genotype ($p = 0.485$) (Figure 3B). This indicates that the response to the 15 min light pulse was not altered in the absence of rods, at least not down to 1 lux light.

Secondly, in the negative masking protocol, a 3 h light pulse applied 2 h after the lights off inhibited locomotor activity (Figure 3C) with a significant light intensity effect ($p < 0.001$) and an interaction between light intensity and genotype ($p = 0.004$). Mutant animals indeed showed reduced masking effect at lowest light intensities ($p < 0.01$ at <1 lux and $p < 0.001$ at 1-10 lux) (Figure 3D).

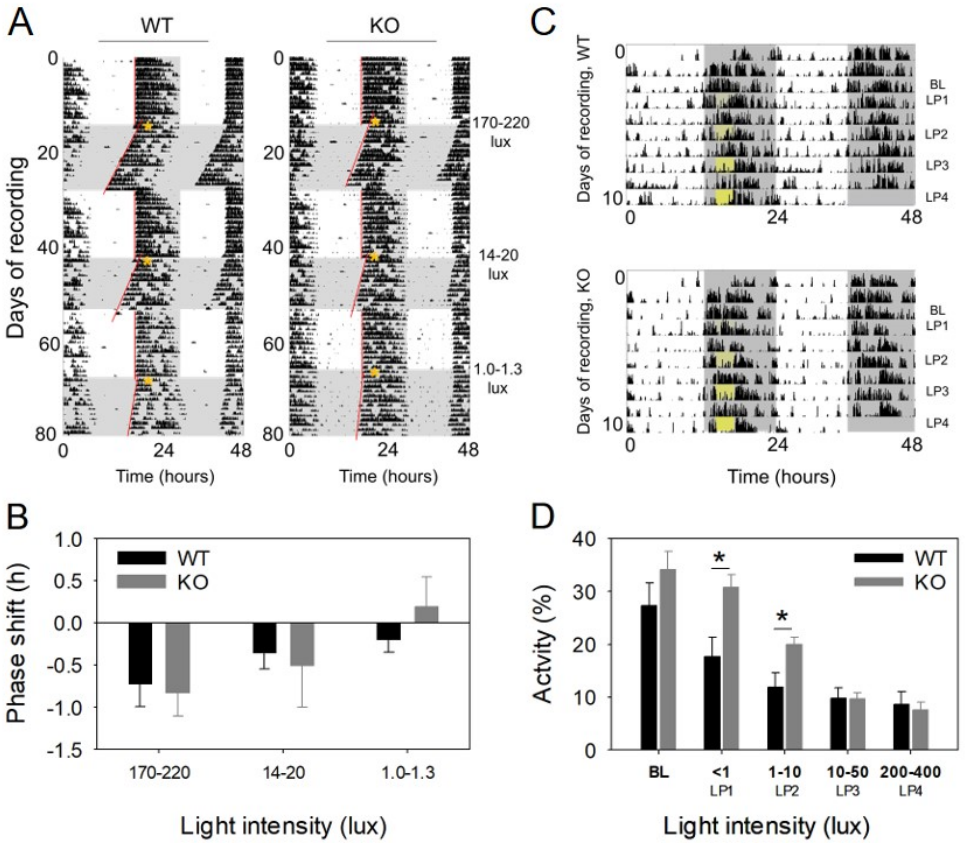

Figure 3: Acute effects of light in Nrl-/- mice

(A) Representative actogram of the wheel-running activity of WT (left) and KO (right) mice following exposure to 15 min light pulses of decreasing intensity given at projected ZT15 (yellow star). Fits to onset of activity used to determine phase shifts are shown in red. Intensities of the pulse are indicated on the right of actograms. (B) Phase delays decreased with light intensity (WT n = 5, KO n = 8; 2-way ANOVA, p = 0.006) but there was no genotype effect (p = 0.251) nor any interaction with light intensity (p = 0.485). (C) Representative actograms of the general locomotor activity of WT (top) and KO (bottom) animals in the negative masking experiment when 3 h light pulses were provided at the beginning of the night phase (ZT14 to ZT17: yellow rectangle) every second day, with increasing light intensities. (D) Residual activity upon light exposure was expressed relative to the total activity during the preceding night ($p < 0.001$) and showed significant interaction between light intensity and genotype (p = 0.004) (WT n = 6, KO n = 7). Post hoc analysis shows significant differences between genotypes for the two lowest stimuli ($p < 0.01$ at <1 lux and $p < 0.001$ at 1-10 lux). Results are represented as mean ± SEM. *: $p < 0.01$. Grey shading indicates darkness.

Figure 3-Source data 1: Raw data of experiments shown in figure 3

Nrl-/- mice do not re-entrain to phase-shifted LD cycle at low light intensity

Animals were challenged with four successive 6 h phase-delayed LD cycles combined with a reduction of light intensity (100 lux, 10 lux, 1 lux, 0,1 lux) (Figure 4A, Figure 4-figure supplement 1). WT animals were able to entrain to each shifted LD cycle at different light intensities while the KO mice needed longer time to entrain at 1 lux (jet-lag 3, $p = 0.026$) and were not able to entrain at 0.1 lux (jet-lag 4, $p < 0.001$) even after 50 days (Figure 4B). Subsequent exposure to total darkness (DD, 22 days) confirmed that almost all mutant animals were free-running in the previous condition (Figure 4A and Figure 4-figure supplement 1; data not shown). When animals were subsequently exposed to LD at 100 lux during the light phase, animals from both genotypes were able to re-entrain (Figure 4B), confirming that there was no overt loss of visual function.

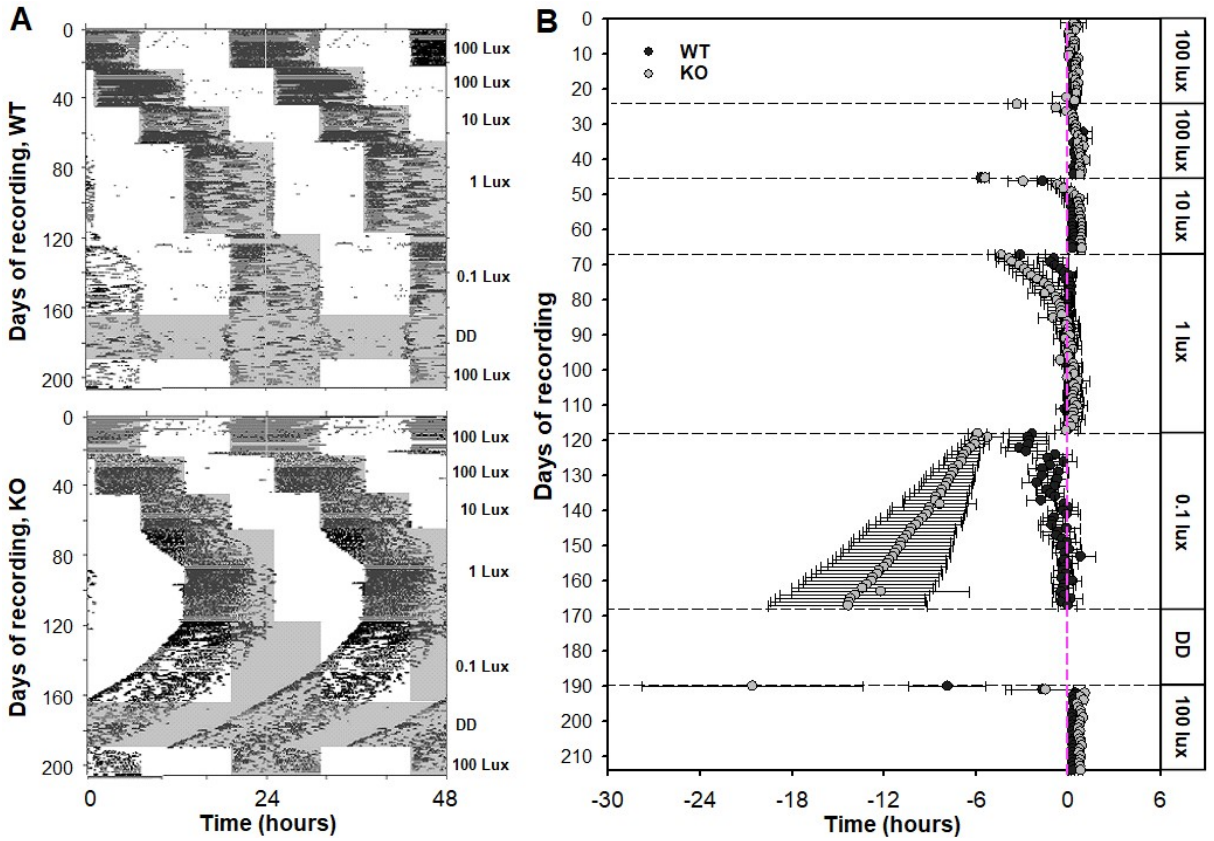

Figure 4: Loss of re-entrainment to a 6 h phase delay at low light intensities in the *Nrl*$^{-/-}$ mice.

Representative actograms from WT (top) and KO (bottom) animals submitted to successive 6h delayed cycles of 12h light and 12h dark with decreasing intensities (indicated on the right side of actograms), then to 22 days of DD and finally again to an LD cycle at normal intensity (100 lux). Grey shading indicates darkness. (B) Onsets of activity expressed relative to ZT0 of the new LD cycle are shown for each day throughout the entrainment experiment, with intensities during the light phase or DD exposure (no data in this case) indicated on the right. *Nrl*$^{-/-}$ animals need more time to re-entrain at 1 lux (p = 0.026) and do not entrain at all at 0.1 lux (p = 0.001) (n = 5 for both WT and KO). Results are represented as mean ± SEM.

Figure 4-Source Data 1: Raw data from experiments shown in figure 4

Figure 4-figure supplement 1: Additional actograms of WT and KO mice in the jet-lag experiment.

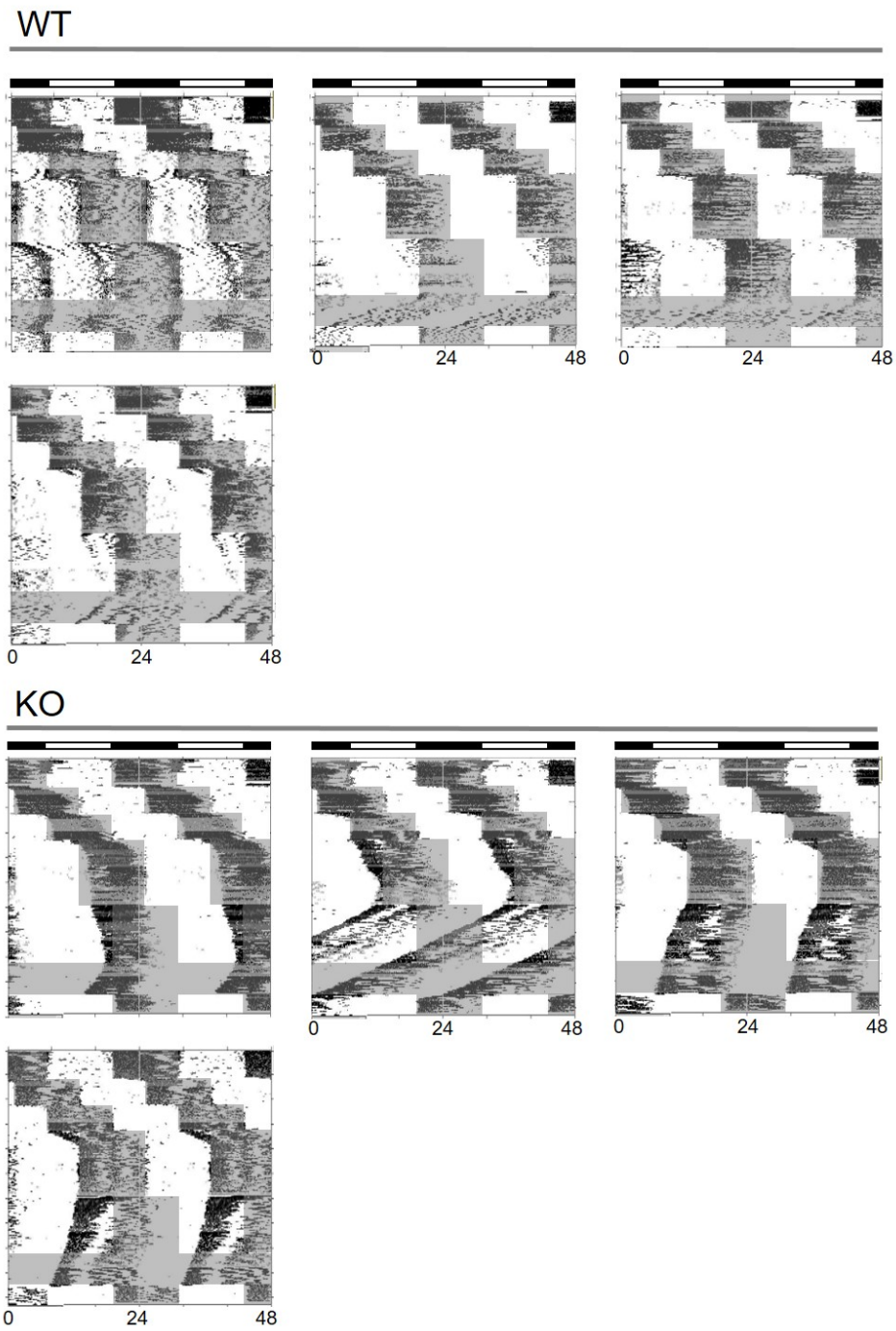

Figure 4-figure supplement 1: Additional actograms of WT and KO mice in the jet-lag experiment.

Wheel-running activity of additional WT and KO mice also used for the analyses presented in Figure 4B.

Major response to constant light in cone only mice

We challenged the mice for 70 days in constant light (LL) (200 lux) (Figure 5A, Figure 5-figure supplement 1). Both genotypes showed rhythmic free-run behaviour but 2 successive steps could be distinguished. A first transient step in which periods substantially increased in both genotypes to approximately 25.5 h and then a stabilized free-run in which periods decreased again, especially in the KO mice (Figure 5B). Thus, 6 out of 7 mutants had periods shorter than 24 h (23.17 ± 0.21 h, $p < 0.015$) while one mutant had a period of 24.17 h. Interestingly, in this interval, KO mice also exhibited almost 8-fold enhanced total locomotor activity ($p = 0.035$) and more than 4-fold increase of the relative rhythmic power ($p = 0.028$) with respect to WT mice (which activity extensively decreased in LL) (Figure 5B, C), indicating a reduced inhibition by light and a higher robustness of the circadian rhythm in the mutant mice. One mutant had arrhythmic locomotor activity during the last 2 weeks in LL When animals were replaced in LD to verify integrity of light responsiveness and activity, mice from both genotypes showed onsets of activity aligned with the start of dark ($p = 1$) (Figure 5A, Figure 5-figure supplement 1) and similar mean activity ratios LD2/LD1 ($p = 0.375$) (Figure 5D).

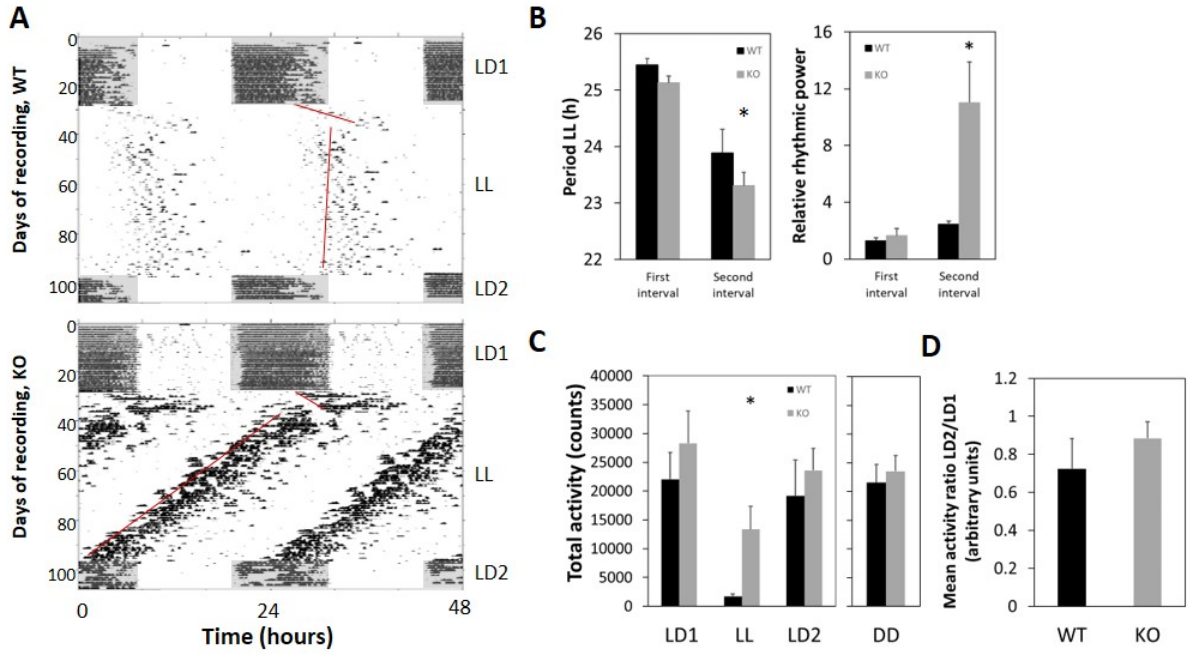

Figure 5: Cone-only mice show perturbed behaviour in constant light

(A) Representative actograms from WT (top) and KO (bottom) animals submitted to 70 days of constant light at 200 lux. Animals were previously maintained in 12h/12h LD cycle (LD1) and returned to the same lighting regime (LD2) following LL conditions. Grey shading indicates darkness. Fits to onset of activity used to determine periods are shown in red. (B) Activity pattern was separated into 2 distinctive intervals of behaviour and thus analysed separately: a first interval with increasing periods for both genotypes and a second one with reducing periods in which the mutant mice exhibited extremely low period values (n = 6 out of 7; $p = 0.015$). Relative rhythmic power was increased in the KO during the second interval ($p = 0.028$). (C) Total activity per cycle was measured in LL (second interval), LD1, LD2 and also compared to the DD condition from Figure 2. Significant difference between WT and mutant mice was observed for total activity specifically during LL ($p = 0.035$). Total activity did not vary for KO animals between lighting regimens ($p = 0.066$) but did for WT between LL and the other lighting conditions ($p = 0.022$). (D) No alterations of activity when animals return to LD, as indicated by similar mean activity ratios LD2/LD1 for WT and KO ($p = 0.375$) (WT n = 6, KO n = 7). Results are represented as mean ± SEM. *: $p < 0.05$.

Figure 5-Source Data 5: Raw data from experiments shown in figure 5

Figure 5-figure supplement 1: Additional actograms of WT and KO mice in constant light condition

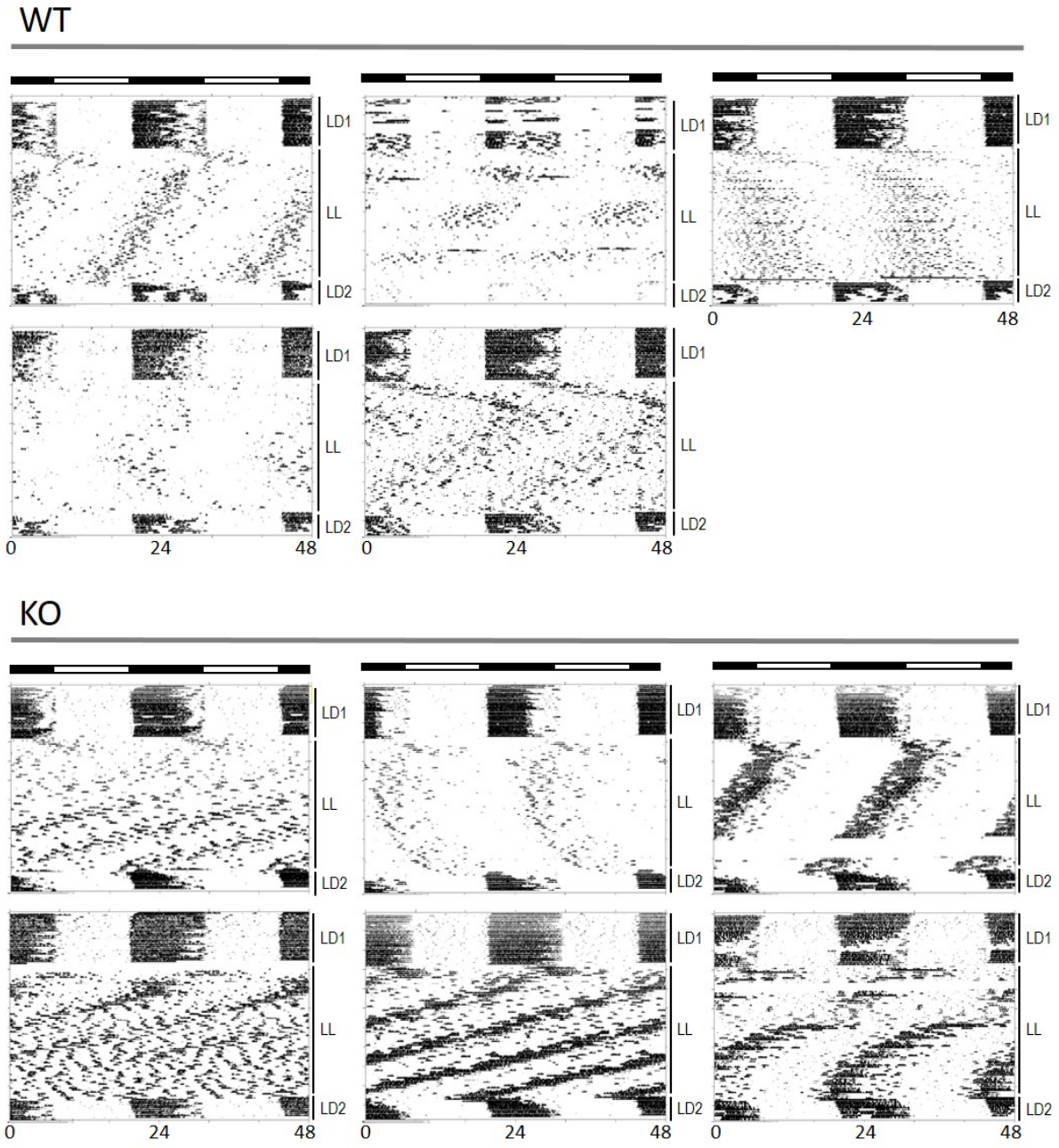

Figure 5-figure supplement 1: Additional actograms of WT and KO mice in constant light condition

Wheel-running activity of additional WT and KO mice also used for the analyses presented in Figure 5B-D.

Discussion

In the present study we used different approaches to determine the role of cones in the circadian system. We show that photoreceptor layers lacking functional rods but having normal cone and cone-pathway contain a molecular machinery characteristic of a functional clockwork and likely contribute, together with the inner and ganglion cell layers, to the overall clock rhythmicity in the retina. We bring evidence that the *Nrl*$^{-/-}$ retina also displays novel distinctive properties regarding light impact on the central clock, providing new insight into the role of cones in the circadian system.

Rhythmic functions in mammalian cones have been only poorly documented (Bobu, Sandu, Laurent, Felder-Schmittbuhl, & Hicks, 2013; Liu et al., 2012; Sakamoto, Liu, Kasamatsu, Iuvone, & Tosini, 2006; Storch et al., 2007; von Schantz, Lucas, & Foster, 1999), likely because of the scarcity of this cell type in nocturnal rodents (Jeon et al., 1998; Szel & Rohlich, 1992). To circumvent this limitation, we used the *Nrl*$^{-/-}$ animal model in which all rods are replaced by cones (Akimoto et al., 2006; Mears et al., 2001). These photoreceptors were previously shown to have major characteristics of native blue cones regarding morphology, molecular content, nuclear architecture and light response (Akimoto et al., 2006; Daniele et al., 2005; Mears et al., 2001; Nikonov et al., 2005) and constitute an adequate model to question the properties of cones without the interference from rods. Moreover, and unlike what was shown in other models with impaired rod phototransduction pathway (Munteanu et al., 2018; Sakamoto, Liu, & Tosini, 2004) these retinas show no sign of alteration of other cellular populations such as dopaminergic amacrine cells, ipRGCs, which are known to contribute to clock properties in the retina (Dkhissi-Benyahya et al., 2013; Liu et al., 2012).

Cellular localization of the circadian clock in the mammalian retina is still a matter of debate. The literature agrees on a main contribution from the inner retina (Jaeger et al., 2015; Ruan et

al., 2008) and several reports exclude rod-type photoreceptors from the circadian network (Baba et al., 2018; Liu et al., 2012; Ruan, Zhang, Zhou, Yamazaki, & McMahon, 2006) although the presence of sustained clock gene rhythms in rods has been suggested elsewhere (Dkhissi-Benyahya et al., 2013; Jaeger et al., 2015; Sandu et al., 2011; Tosini, Davidson, Fukuhara, Kasamatsu, & Castanon-Cervantes, 2007). Upon immunofluorescence analysis of clock protein factors, cones appeared the most evident cell-autonomous clock in the mouse retina (Liu et al., 2012). In agreement with this study, we here describe robust rhythms in expression of clock genes from the main (*Bmal1*, *Per1*, *Per3*) and secondary (*Rev-Erbα*) loops of the well described molecular machinery (Takahashi, 2017) in $Nrl^{-/-}$ photoreceptor layers laser-microdissected throughout the 24 h cycle in constant dark condition. However, unlike what was described for immunostained clock factors, their mRNAs show distinct phases, as observed at the level of the whole retina (Ruan et al., 2008), which might be due to the enrichment in S- versus M-cones in the KO retinas or suggest post-transcriptional regulation of clock factors. We previously described that cones are the photoreceptor site of robust oscillations in *Aanat* (the enzyme responsible for melatonine rhythm) expression by using a diurnal, cone-rich rodent, *Arvicanthis ansorgei* (Bobu et al., 2013; Gianesini et al., 2015). Besides, circadian rhythms in cone-specific genes have essentially been investigated in chicken (Haque et al., 2010; Pierce et al., 1993) and zebrafish (P. Li et al., 2008). In particular, robust rhythms in phototransduction genes in zebrafish cones appear driven by key transcription factors (*Neurod*, *Crx*) themselves regulated by the clock (Laranjeiro & Whitmore, 2014). In our study, cones express major phototransduction elements in a rhythmic manner with high amplitudes but we did not detect any rhythm in *Crx* expression, indicating that in mammalian cones phototransduction elements retain clock regulation but with mechanisms distinct from the zebrafish. Importantly, when isolated by vibratome-sectioning of fresh retinas, cone layers express sustained rhythms with a specific period, distinct from the period measured in photoreceptor layers from control mice. This observation probably reflects

457 the differences in clock machinery and associated signalling occurring in rods (97% of
458 photoreceptors in WT) versus cones. It might also reflect a difference in coupling strength
459 within the respective photoreceptor populations, as previously described in the retina (Jaeger
460 et al., 2015). Communication through gap junctions might be reduced in the S-cone enriched
461 photoreceptor layers of the KO, since expression of connexion 36 was shown to be absent in
462 this cone population in mammals (W. Li & DeVries, 2004). This might be responsible for the
463 increased period in the KO (Jaeger et al., 2015). Taken together with our demonstration of
464 rhythmic phagocytosis of cone outer segments (Krigel et al., 2010) our data strongly suggest
465 the presence of a functional, autonomous circadian clock within cones.
466
467 To get more insight into the contribution of cones to the retinal clock network we turned to an
468 imaging-coupled bioluminescence approach. Bioluminescence imaging of transversal retinal
469 sections shows rhythmic *Per2* expression throughout the (cone) outer nuclear layer,
470 confirming that cones contribute to the retinal clock network, even if this is low when
471 compared to the signal displayed by the ganglion cell and inner nuclear layers. The
472 observation that the three cell layers of the retina show similar, >25 h periods further fits with
473 our previously described model of multi-oscillatory retinal clock (Jaeger et al., 2015). By
474 contrast, when considering bioluminescence in whole retinal explants, the replacement of rods
475 by cones leads to substantial reduction in baseline and amplitude without any effect on the
476 period, rhythmic power and damping rate. This result is unexpected in regard of recent
477 literature reporting the absence of clock in rods (Baba et al., 2018; Ruan et al., 2006) and does
478 not exclude that the rod population does contain a clock and contributes to the oscillator
479 network in whole retinas. It cannot be excluded, however, that the defects in the *Nrl*$^{-/-}$ retinas
480 reflect the health status of their photoreceptors, even if sampling was done prior to their
481 reported apoptosis period (Roger et al., 2012).
482

The involvement of cones in circadian functions has been substantially documented. A role in synchronisation of the SCN has been demonstrated for both green cones (Dkhissi-Benyahya et al., 2007) and S-cones (Provencio & Foster, 1995; van Diepen et al., 2013; van Oosterhout et al., 2012; Walmsley et al., 2015). However, the contribution of cones to the effects of white ambient lighting on circadian properties and more generally non-image forming vision, has been evaluated with a limited variety of visually impaired mouse models. We used a battery of behavioural tests (Hughes, Jagannath, Hankins, Foster, & Peirson, 2015) to investigate this question with the cone-only *Nrl*$^{-/-}$ model. Our data were generated in indoor laboratory conditions comprising full spectrum visual light in agreement with the capacity of the KO model to respond to photopic light similar to the WT upon electroretinography recording (Figure 2-figure supplement 1). We observed that the high number of cones does not provide any increased response capacity of the circadian system to the diverse light stimulation paradigms used here. This result corroborates previous discussion in the field, suggesting that the light adaptation properties of cones preclude their participation in the input of long light exposure to the circadian system, including phase shift experiments (Altimus et al., 2010; Lall et al., 2010). Indeed, no defect was detected in *Nrl*$^{-/-}$ mice under the phase shift paradigm (as also seen in (Calligaro et al., 2019)). By contrast, our model rather displays some features typical of rodless animals, such as reduced capacity to shift at low light intensity (1 or 0.1 lux) in a jet-lag experiment, as previously observed with the *Gnat1*$^{-/-}$ model (Altimus et al., 2010). Physiological features of rodless retina are also reflected in dopamine metabolism (Figure 1-figure supplement 2D), with the loss of daily rhythm of DOPAC generation in KO retinas (Nir & Iuvone, 1994; Perez-Fernandez et al., 2019) as previously described for the rds strain. The discrepancy between the results from light pulse and the jet-lag experiments might be due to the fact that the threshold levels required for entrainment constitute a more sensitive test of deficit in entrainment than phase shift following a light pulse (Mrosovsky, 2003).

509 Rats or mice with outer retinal impairment were repeatedly reported to exhibit total loss of
510 positive masking by light and (consequently) enhanced inhibition of locomotor activity
511 (negative masking), especially at low light intensities (Mrosovsky, Foster, & Salmon, 1999;
512 Thompson et al., 2010; Thompson et al., 2011). By contrast, melanopsin phototransduction
513 appears indispensable for negative masking (Mrosovsky & Hattar, 2003). Using
514 monochromatic light, Thompson et al. also provide evidence that cones (short- and medium-
515 wavelength sensitive) contribute to negative masking and influence its dynamic range
516 (Thompson, Foster, Stone, Sheffield, & Mrosovsky, 2008). In the present study, the *Nrl*$^{-/-}$
517 animals show reduced negative masking behaviour specifically at low light intensities
518 (between 0.5 and 10 lux), despite a normal ipRGC population and unlike most rodless mice.
519 The discrepancy between this result and the literature might be explained by the fact that we
520 used global activity recordings and not wheel running activity. Indeed, positive masking
521 might be more pronounced when using wheel running activity and hence introduce a
522 confounding effect (increased negative masking in rodless animals) at low light intensity.
523 Furthermore, some data also indicate that rods contribute, at least transiently, to negative
524 masking at light intensities too low to excite ipRGC (Butler & Silver, 2011). Thus, the
525 behaviour triggered in the *Nrl*$^{-/-}$ animals by acute light stimulation probably reflects the
526 combined absence of rods and integrity of ipRGC.
527
528 Increase of the endogenous period in constant light has also been partly attributed to rod
529 signalling (Altimus et al., 2010; Lall et al., 2010) and requires the integrity of ipRGC (Goz et
530 al., 2008). In our experiments we observed that the free running periods in LL were first
531 increased to a similar extent for both the WT and mutant mice, suggesting that mechanisms
532 distinct of the rod-pathway are involved. However, periods then decreased, with WT reaching
533 a mean value around 24 h and the mutants rather lower periods (23.25 h on average). In
534 addition, KO mice exhibit particularly high (around 8-fold increase with respect to the WT)

level of activity, indicating loss of masking by constant light, a feature which is also shared with mice devoid of ipRGC (Goz et al., 2008). However, upon re-exposure to a standard 12 h:12 h LD cycle after the LL, both WT and KO mice re-entrained very rapidly, suggesting that there was no major impairment of the circadian photosensitivity. Short free-running period values have been rarely described in LL, except in *Per2* clock gene mutants of different backgrounds (Pendergast, Friday, & Yamazaki, 2010; Spoelstra & Daan, 2008; Steinlechner et al., 2002). The phenotype in the *Nrl*$^{-/-}$ mice could be explained by distinct hypotheses: 1, their high wheel running activity in LL might feedback on the clock and induce period shortening (Edgar, Martin, & Dement, 1991); 2, cone abundance could trigger another, yet unknown signalling towards the central clock. Identification of the mechanisms by which excess of cones alters properties of the circadian system will require further investigation.

In conclusion, by using the *Nrl*$^{-/-}$ cone-only mouse model we provide compelling evidence that cones contain a circadian clock part of the retinal oscillating network. Although *Nrl*$^{-/-}$ mice do not exhibit overt dysfunction of circadian behaviour, their exposure to specific experimental paradigms highlights their particularities, namely properties induced by the absence of rods or, importantly, specific to the enlarged cone population and revealed by exposure to constant light. Taken together with results from other studies, our data confirm the interest of visual system mutants in the understanding of retinal pathways regulating the central clock.

Materials and methods

Animals

Mice were handled according to the French Law implementing the European Union Directive 2010/63/EU. All procedures involving the use of mice were approved by the Animal Use and Care Committee from Strasbourg (CREMEAS). *Nrl*$^{-/-}$ (C57Bl/6J background) mice were obtained from Dr. C. Grimm (Laboratory of Retinal Cell biology, University Hospital Zurich, Switzerland) with permission from Dr. A. Swaroop (NEI, Bethesda, MD, USA) (Mears et al., 2001). *mPer2*^{Luc} mice (Yoo et al., 2004) (C57Bl/6J background, previously purchased from The Jackson Laboratory, Bar Harbor, ME, USA) were crossed with *Nrl* mutants to generate the *Nrl*$^{-/-}$ *Per2*^{Luc} and *Nrl*$^{+/+}$ *Per2*^{Luc} animals. According to experiments, WT (*Nrl*$^{+/+}$) and KO (*Nrl*$^{-/-}$) animals were either homozygous for the *Per2*^{Luc} knock-in allele (stated *Per2*^{Luc} background) or did not contain *Per2*^{Luc} allele. All the mice were raised in the Chronobiotron animal facility (UMS 3415, Strasbourg, France) and housed in standard cages in groups of 3 to 4 individuals, under 12h:12h light-dark (LD) cycles [ZT0-light on, ZT12-light off; broad spectrum (400-650 nm) white light at 300 lux (MASTER PL-L 4 lamp, Philips, France); no red light at night] with food and water *ad libitum* and in an ambient temperature of 22 ± 1°C. Experiments were performed on both males and females unless otherwise stated. In most cases, no a priori estimation of sample size was performed. Our groups were based on previous or preliminary data and tried to conform to the 3R rule.

Laser microdissection

Six week-old *Nrl*$^{-/-}$ males (n = 30) reared in LD were exposed to constant dark (dark/dark, DD; no dim red light). After 36 h in DD mice were euthanized within the following 24 h in DD in a CO_2 (up to 20%) airtight chamber at the following projected ZT time points: 0, 4, 8, 12, 16, 20 (n = 5, randomly allocated, per time point). Eyes were enucleated, embedded in

Tissue-Tek OCT compound (Sakura Finetek USA, Torrance, CA), frozen on dry ice and stored at −80°C until use. Animal handling and eye sampling were performed by using night vision goggles (ATN NVG-7, ATN-Optics, Chorges, France).

20 µm thick eyeball sections were cut on cryostat and placed on polyethylene naphthalate (PEN) Membrane Frame slides (Life Technologies, Grand Island, NY). Three to four slides (4 sections/slide) were prepared from a single eye specimen. Each slide was stored at −80°C in a 50 mL nuclease-free tube (pre-chilled on dry ice) and used for laser microdissection within a week.

Frozen slides were thawed at room temperature for 30 s. Sections were stained with cresyl violet (1% cresyl violet acetate in 70% ethanol) for 30 s, then dehydrated through a series of ethanol solutions: 2 x 75% for 30 s, 95% for 30 s, 100% for 30 s and 100% for 2 min. Slides were air dried at room temperature for 1 min then completely dehydrated in a vacuum chamber for 1 h before microdissection. The whole procedure was performed in RNase free conditions.

Laser microdissection was performed using the Veritas Microdissection Arcturus system and software (Arcturus Bioscience, Inc. Mountain View, CA, USA) immediately after complete dehydration of the slides. The cone photoreceptor areas of interest were selected under microscope (20x magnification) and transferred on CapSure Macro LCM Caps (Life Technologies, Grand Island, NY) by the combined use of the infrared (power 70-80 mW, pulse 1500-3500 µs) and UV (low power 2-4) lasers (See also Figure 1A). A total cone photoreceptor area of 3 mm^2 was collected per eye. In order to prevent RNase reactivation and RNA degradation, the microdissection was carried out within maximum 60 min for each slide. 3-4 caps/eye were collected into the same reaction tube which contained RLT^+ lysis buffer (Qiagen, Hilden, Germany) and stored at −80°C.

Quantitative reverse-transcription PCR

Total RNA was extracted from the microdissection lysates using RNeasy Plus Micro kit (Qiagen, Hilden, Germany) according to the manufacturer's instructions and eluted in a final volume of 12 µL. RNA quantity and purity were measured using the Nanodrop ND-1000 spectrophotometer (Thermo Scientific, Wilmington, DE, USA). RNA integrity was assessed with the 2100 Bioanalyzer (Agilent Technologies, Santa Clara, CA, USA) and the RNA 6000 Pico chips (Agilent Technologies, Santa Clara, CA, USA), following the manufacturer's instructions. 25 ng of RNA from samples with the RNA integrity number (RIN) > 6 (n = 3-5) were amplified using ExpressArt mRNA amplification Nano kit (Amsbio, Oxon, UK). 150 ng of amplified RNA was reverse transcribed by using the iScript™ Advanced cDNA Synthesis Kit for RT-qPCR (Bio-Rad, Hercules, CA, USA) in a final volume of 20 µL. All samples were stored at −80°C.

500 ng total RNA extracted from whole retinas of 4-month old mice (n = 7 WT, n = 8 KO; euthanasia at ZT7-8 by CO_2) were reverse transcribed using the High capacity RNA-to-cDNA Kit (Applied Biosystems, ref# 4387406).

Transcript levels were determined by quantitative PCR as described (Sandu et al., 2011), with PCR reactions run in duplicates. The purity of the microdissected samples was verified by the absence of detection by qPCR, of transcripts for tyrosine hydroxylase (*Th*) gene and metabotropic glutamate receptor 6 (*mGluR6*) gene, as markers for the inner nuclear layer. Transcript levels were normalized to the levels of *Tbp* and *Hprt* which showed constant expression in the isolated cones over the 24 h (data not shown). Transcript levels in whole retinas were normalized to the levels of *Gapdh* and *Hprt* which did not vary between genotypes (data not shown). All TaqMan probe-based assays were purchased from Applied Biosystems (Applied Biosystems, Foster City, CA, USA) and designed to span exon boundaries (Table 2). Data was quantified using the ΔCq method, modified to take into

account gene-specific amplification efficiencies and multiple reference genes, and the qBase software (free v1.3.5) (Hellemans, Mortier, De Paepe, Speleman, & Vandesompele, 2007). In microdissected cones, log transcript levels were calculated relative to the transcript levels measured in a WT photoreceptor sample which were rescaled to one. We used Excell software to detect outliers which were removed for the final statistical analysis (n = 1 for *Per1*, *Per2* and *Per3* quantification).

Real-time bioluminescence recordings

Bioluminescence recordings from whole retinas and isolated photoreceptor layers were obtained in several successive experiments and data were analysed all together. Only samples generating a bioluminescence signal above the background level were retained in the study.

Whole retina explant cultures

WT and KO mice (5-6 week-old, *Per2*^{Luc} background), were euthanized with CO_2 (progressive increase up to 20% in an airtight box) during the light phase and enucleated. Eyeballs were kept at room temperature in HBSS [1 x HBSS (Sigma-Aldrich, Steinheim, Germany) containing antibiotics (100 U/mL penicillin and 100 mg/ml streptomycin, Sigma-Aldrich, Steinheim, Germany), 100 mM HEPES (Sigma-Aldrich, Steinheim, Germany) and 4.2 mM sodium bicarbonate (Sigma-Aldrich, Steinheim, Germany)] for whole retina dissection. The eye ball was incised under the ora serrata and the cornea and lens were cut out. Retinas were carefully detached from the retinal pigment epithelium and flattened with small radial incisions.

Each flattened retina was placed, photoreceptors down, onto a semipermeable membrane (Millipore, Billerica, MA, USA) in a 35 mm culture dish (Nunc, ThermoFisher, France) containing pre-incubation medium [1 ml neurobasal A medium (Gibco, Invitrogen, Life Technologies, Carlsbad, CA, USA) supplemented with antibiotics (25 U/ml penicillin and 25

mg/mL streptomycin, Sigma-Aldrich), 2% B27 (Invitrogen, Life Technologies, Grand Island, NY, USA), and 2 mM L-glutamine (Gibco, Life Technologies, Carlsbad, CA, USA). Samples were kept 24 h at 37°C in a humidified 5% CO_2 incubator then the medium was changed with pre-warmed (37°C) 199 recording medium [1 mL medium 199 (Sigma-Aldrich, St. Louis, MO, USA) supplemented with antibiotics (25 U/mL penicillin and 25 mg/mL streptomycin, Sigma-Aldrich), 4 mM sodium bicarbonate, 20 mM D(+)-glucose (Sigma-Aldrich), 2% B27 (Invitrogen), 0.7 mM L-glutamine (Gibco), and 100 mM beetle luciferin (Promega, Fitchburg, WI, USA). The medium change was performed under dim red light. Dishes were sealed with high-vacuum grease (Dow Corning; Midland, MI, USA) and placed into the LumiCycle (Actimetrix, Wilmette, IL, USA) heated at 36°C. Samples were recorded during 6-8 days and the photons were integrated for 112 s every 15 min. In bioluminescence recordings, the 2 retinas from the same animal are considered as independent, biological replicates. We here analysed n = 12 (8 mice) for WT and n = 12 (7 mice) for KO.

Photoreceptor layer explant cultures

Retinas were dissected as described above. Photoreceptor layers were isolated using the vibratome technique and cultured as reported previously (Jaeger et al., 2015). WT (n = 6 samples, 6 mice) and KO (n = 9 samples, 8 mice) photoreceptor explants were recorded for at least 5 days and the photons were integrated for 112 s every 15 min. Exceptionally, when layers of insufficient size were collected, samples from both retinas were cultured together (2 samples in WT group, 1 sample in KO group).

Transversal retinal slice imaging

Flattened retinas (4 week-old KO mice, n = 3, *Per2*^{Luc} background) were mounted with warm (37°C) 5% gelatin on top of a 10% gelatin block. The whole retina-embedded block was

glued on the tissue holder and then placed into the tissue bath (containing HBSS, Sigma-Aldrich) of a Vibroslice MA752 (Campden Instruments, Loughborough, England). A transversal 100 µm thick slice was cut, placed carefully on a semipermeable membrane in a 35 mm culture dish and pre-incubated with neurobasal A medium for 24 h. Just before imaging the medium was replaced with pre-warmed recording medium under dim red light. The sealed dish was placed into the culture chamber (37°C) of a Luminoview 200 microscope (Olympus, Hamburg, Germany) equipped with an EM-CCD camera (Hamamatsu, Japan) cooled to −76°C. Bioluminescence images (20x objective, EM gain = 80, 1 × 1 binning of pixels) were taken every 2 h over minimum 3 days.

SCN bioluminescence recordings

Animals (9 month-old, WT n = 5, KO n = 7, *Per2*^{Luc} background) were killed by cervical dislocation and brains were rapidly removed and placed in ice-cold HBSS. One 500µm coronal section of the SCN region was obtained using a stainless steel adult mouse brain slicer matrix (ZIVIC Instruments, Pittsburgh, USA), then trimmed to 1 × 1 mm. Each SCN explant (containing both nuclei) was cultured onto a Millicell culture membrane (Merck Millipore Ltd, Tullagreen, Ireland) in a 35-mm culture dish with 1 mL of DMEM (Sigma-Aldrich) supplemented with 0.35% D(+)-glucose, 0.035% sodium bicarbonate, 10 mM HEPES, 2% B27, antibiotics (25U/mL penicillin and 25mg/mL streptomycin) and 0.1 mM beetle luciferin. Culture dishes were sealed with vacuum grease. The bioluminescence was recorded using the LumiCycle for 112 s in 15 min intervals and during at least 6 days.

Bioluminescence data analysis

Whole retina and SCN explant PER2::LUC raw data were subtracted with a 24 h running average (removal of the baseline drift) using the LumiCycle analysis software (Actimetrics, Wilmette, IL, USA). The first cycle was removed and the analysis was performed on the

following 4 (retina) or 5 (SCN) cycles. The robustness of the rhythms (relative rhythmic power (Klarsfeld, Leloup, & Rouyer, 2003)) and the phase were also calculated using the LumiCycle analysis software. The period, amplitude and damping rate were determined using a cosinor derived sine wave function: $f = y0 + a * \exp(-x/d) * \sin[2 * \pi * (x + c) / b]$ where a is the amplitude (counts/s), b is the period (h), c is the phase-related term (h) and d is the damping rate (days) and assuming that damping follows an exponential pattern. Baseline for each individual peak in retinal samples was estimated as the baseline from LumiCycle analysis taken at the peak time.

Photoreceptor layer data were analyzed as previously described, on 4 successive cycles (Jaeger et al., 2015).

Bioluminescence data from whole retinas and photoreceptor layers were obtained over several series of recordings: samples for which activity did not exceed the background of Lumicycle were excluded from the study

Transversal retinal images were analyzed with ImageJ (open source software https://imagej.nih.gov/). A median 3D filter was applied to remove the hotspots. The ganglion cell layer (GCL), inner nuclear layer (INL) and photoreceptor layer (PRL) were defined as regions of interest (ROI) and the bioluminescence levels (grey levels) were measured and exported for the analysis of rhythmicity. The periods were determined using the cosinor derived sine wave function: $f = y0 + a * \exp(-x/d) * \sin[2 * \pi * (x + c) / b]$ as above.

Retina whole-mount immunohistochemistry

Immunohistochemical staining was performed on whole retinas obtained from 6-8 week-old *Nrl*$^{-/-}$ *Per2*^{Luc} mice (WT n = 5, KO n = 6). Eyes were sampled by enucleation from mice euthanized between ZT3 and ZT6 by cervical dislocation and immediately fixed in 4%

paraformaldehyde for 2 h at room temperature (RT). Retinas were dissected and flattened by four incomplete radial incisions made at roughly equal spacing. Free floating retinas were blocked in 10% normal donkey serum (NDS), 1% Bovine Serum Albumin (BSA), 0.5% Triton X-Phosphate Buffered Saline (Tx-PBS) for 3 h at RT and subsequently incubated 5 days under gentle agitation in 3% NDS, 1% BSA, 0.5% Tx-PBS and 0.05% Sodium azide at 4°C with primary antibodies: polyclonal anti-melanopsin (OPN4) antibody (clone AF006, Advanced Targeting System; 1:4000), as previously published in (Provencio, Rollag, & Castrucci, 2002) and polyclonal anti-Tyrosine Hydroxylase (TH) (reference AB1542 Millipore; 1:4000). Retinas were washed extensively in PBS (6 x 30 min at RT), and incubated with Alexa secondary antibodies (Invitrogen; 1:1000) 3 h at RT. After washing the secondary antibodies (6 x 30 min at RT), retinas were mounted with Fluoromount-G (Southern Biotech) to prevent photobleaching. Retinal whole-mount fluorescent images were obtained using an Axio Imager 2 microscope for mosaic imaging (Zeiss; 10x objective) at identical exposure times between WT and KO specimens. Quantification was performed by counting the total numbers of OPN4 and TH positive cells on the photographs using the Adobe Photoshop CS6 software (no image treatment was done).

HPLC measurements

4 months-old mice (n = 6 per genotype group and per time point, randomly allocated) were euthanasized by CO_2 (20%) at ZT4 and ZT16 and retinas were rapidly extracted after slitting the cornea with a sterile scalpel blade and discarding the lens and vitreous. Retinas were quickly frozen on dry ice and stored at -80°C. Frozen retinas were homogenized by ultrasonication in 0.4M $HClO_4$. Samples were centrifuged (13 000 rpm) for 20 minutes, and supernatants were analyzed for dopamine and 3,4-dihydroxyphenylacetic acid (DOPAC) with an HPLC system (Decade II Antec). Standard solution of dopamine and DOPAC (Sigma-

752 Aldrich) were diluted in the same mobile phase in order to obtain a 3-point standard curve for
753 each standard for the quantification of the samples.
754
755 **Electroretinography**
756 Electroretinography was used to assess visual sensitivity of *Nrl*$^{-/-}$ mice in the visible spectrum
757 using the RETI port / scan 21 setup (Stasche & Finger GmbH, Roland Consult, Brandenburg,
758 Germany) as previously reported (Ait-Hmyed Hakkari et al., 2016). All recordings were
759 obtained around the middle of the animal's light phase between projected ZT5 and ZT7. Dark-
760 adapted mice (n=5 for WT, n=3 for KO) were anesthetized by subcutaneous. injection of
761 ketamine (50 mg/kg; Imalgène 1000; Merial, Lyon, France) and xylazine (10 mg/kg; Rompun
762 2%; Bayer, Puteau, France). Pupils were dilated with 0.5% Tropicamide (Ciba Vision
763 Ophthalmics, Blagnac, France). Animals were then placed on a warming plate to maintain a
764 constant body temperature, and ground, reference, and corneal electrodes (thin gold wire with
765 a 2-mm ring end) were placed accordingly. Eyes were kept moist with eye drops (Ocry-Gel;
766 TVM Lab, Lempdes, France). Mice were then exposed to a rod-saturating white light
767 background (40 cd/m^2) inside the Gansfeld bowl. After 10 min of light-adaptation, single-
768 flash photopic ERG recordings were performed successively at specific wavelengths 455 and
769 525 nm and then under white light, at 1, 3 and 10 cd.s/m^2 (6 flashes per intensity). Amplitudes
770 of a and b-waves were analyzed off-line: only the b-wave was measurable for photopic ERG.
771
772 **Locomotor activity recordings**
773 For behavioural recordings, male and female mice (WT and KO combined or not with the
774 *Per2*^{Luc} knock-in allele) were housed in individual standard cages equipped with a 10-cm-
775 diameter stainless steel running wheel (Mendoza, Graff, Dardente, Pevet, & Challet, 2005) or
776 with infrared detectors placed above the cage and linked to an automated recording system

(CAMS, Circadian Activity Monitoring System, Lyon, France) as previously described (Salaberry, Hamm, Felder-Schmittbuhl, & Mendoza, 2019). Data were collected in 5 min bins and analysed with the ClockLab Software (Actimetrics, Wilmette, IL, USA). Locomotor activity data were double-plotted in actograms.

Circadian phenotype

To determine the daily and circadian rhythm of locomotor activity in *Nrl* mutant mice, 5-6 month-old mice (WT n = 4, KO n = 7, *Per2*^{Luc} background) were initially maintained for 12 days under LD 12:12 and then 19 days under constant darkness (DD). Total activity and *rho*- and *alpha*-phase activity levels were calculated during LD and the endogenous period (Chi-square Periodogram method) was determined over 10-day interval after 7 days from the transition to DD.

Behavioural phase-shifts to light pulses

To evaluate phase shifting in response to light pulses 5-6 week-old mice (WT n = 5, KO n = 8) were initially maintained in LD 12:12 (100 lux) and then challenged by 3 alternating DD (9-14 days) - LD (14-18 days) cycles. On the day before each light-pulse, the room lights went off at ZT12. On the following day a 15 min light pulse (LP) was applied at the projected ZT15. Then lights remained off for at least 9 days before re-exposing animals to LD condition. The intensity of the light pulses decreased one order of magnitude as indicated in Figure 3A, B. To determine phase changes in control and *Nrl* mutant mice, a linear regression analysis of the activity onsets was performed by projecting the onset phase of the free run in DD back to the mean onset phase under LD condition (ClockLab).

Masking

To evaluate the negative masking response to light, 3-6 month-old mice (WT n = 6, KO n = 7, *Per2*^{Luc} background) mice adapted to 12:12 LD cycle were housed in individual cages into a

ventilated cabinet (Charles River Laboratories, France) equipped with broad spectrum white light lamp (MASTER TL-D Super 80 lamp, Philips). The masking effect of light was tested by exposing the animals to light for 3 hours from ZT14 to ZT17 at successive light intensities as follows: day 1 (baseline) - standard 12:12 LD; day 2 – ZT14-17 at <1 lux; day 4 – ZT14-17 at 1-10 lux; day 6 – ZT14-17 at 10-50 lux; day 8 – ZT14-17 at 200-400 lux; days 3, 5, 7 – standard 12:12 LD. Locomotor activity was monitored with infrared cage top motion sensors connected to the CAMS data acquisition system (Circadian Activity Monitoring system, INSERM, Lyon, France) (Dkhissi-Benyahya et al., 2007). The percent of activity during the 3 h light pulse was calculated relative to the 12 h activity of the preceding standard night.

Re-entrainment to 6-h light–dark cycle delay

1.5-3 month-old mice (WT n = 5, KO n = 5) were kept for 23 days in LD at 100 lux (LD1) and then challenged with 4 successive 6-h phase delays, mimicking a jet-lag (JL) or cycle change across six time zones, combined with reduction of light intensity: JL1 (21 days, 100 lux), JL2 (22 days, 10 lux), JL3 (51 days, 1 lux) JL4 (50 days, 0,1 lux). At the end of the last JL exposure, animals were transferred to DD (22 days) and then re-exposed 25 days to LD at 100 lux (LD2). The phase angle of entrainment was determined by calculating the difference between the time of lights off and the time of activity onset (ClockLab).

Exposure to constant light

We tested the effects of constant light exposure (light/light, LL) on cone-only animals by assessing wheel running activity in 6 month-old mice (WT n = 6, KO n = 7**,** *Per2*^{Luc} background). Thus**,** after 10 days in LD 12:12 animals were transferred to LL for 70 days at 200 lux. Total activity per cycle, period and relative rhythmic power were measured by using ClockLab. Mice were then exposed to a second LD cycle (LD2: 10 days) to evaluate if entrainment and locomotor activity returned to baseline levels.

Statistical analysis

Results are expressed as means ± SEM, except for qPCR data. Statistical analyses were performed by using SigmaPlot 12 software (Systat Software, San Jose, CA, USA). Comparison of two groups was performed by using the Student's t test. Comparison of several groups was performed by using 1-way or 2-way ANOVA for independent and repeated measures, followed by post hoc test (Holm-Sidak test).

Data from qRT-PCR over 24 h in DD were also analyzed by nonlinear least-square fitting of a 24 h sinusoid (cosinor analysis) $f = a + [b*\cos(2* \pi *(x - c) / 24)]$ (Nelson, Tong, Lee, & Halberg, 1979). A posteriori Power analysis was also performed and is presented in Figure 1-figure supplement 1.

A statistically significant difference was assumed with *p* values less than 0.05.

838

Gene	TaqMan assay reference	RefSeq	Exon boundary	Assay location	Amplicon length (bp)
Bmal1	Mm00500226_m1	NM_001243048.1	8-9	900	87
Clock	Mm00455950_m1	NM_001289826.1	15-16	1548	81
Per1	Mm00501813_m1	NM_001159367.1	18-19	2628	106
Per2	Mm00478113_m1	NM_011066.3	19-20	3271	73
Per3	Mm00478120_m1	NM_001289877.1	4-5	1027	73
Cry1	Mm00514392_m1	NM_007771.3	1-2	740	64
Cry2	Mm00546062_m1	NM_009963.4	1-2	255	70
Rev-Erbα	Mm00520708_m1	NM_145434.4	1-2	664	62
Rorβ	Mm00524993_m1	NM_001043354.2	2-3	730	74
Opn1sw	Mm00432058_m1	NM_007538.3	4-5	1017	64
Opn1mw	Mm00433560_m1	NM_008106.2	4-5	771	87
Opn4	Mm00443523_m1	NM_001128599.1	1-2	327	88
Crx	Mm00483994_m1	NM_007770.4	1-2	141	74
c-Fos	Mm00487425_m1	NM_010234.2	1-2	279	59
Tbp	Mm00446971_m1	NM_013684.3	2-3	305	93
Hprt	Mm01545399_m1	NM_013556.2	2-3	276	81
Gapdh	Mm99999915_g1	NM_001289726.1	2.3	276	81
MGluR6	Mm00841148_m1	NM_173372.2	9-10	2273	67
Th	Mm00447557_m1	NM_009377.1	12-13	1340	61

839

840 **Table 2: References of the TaqMan probes (Applied Biosystems, Life**

841 **Technologies) used for real-time PCR.**

Acknowledgements

We thank Dr. Dominique Sage, Dr. Sophie Reibel and Nicolas Lethenet from Chronobiotron UMS 3415 (Strasbourg, France) for animal care, Dr. Anand Swaroop for the *Nrl* KO mice and Daniel Clesse for HPLC measurements.

References

Ait-Hmyed Hakkari, O., Acar, N., Savier, E., Spinnhirny, P., Bennis, M., Felder-Schmittbuhl, M. P., . . . Hicks, D. (2016). Rev-Erbalpha modulates retinal visual processing and behavioral responses to light. *FASEB J, 30*(11), 3690-3701. doi:10.1096/fj.201600414R

Akimoto, M., Cheng, H., Zhu, D., Brzezinski, J. A., Khanna, R., Filippova, E., . . . Swaroop, A. (2006). Targeting of GFP to newborn rods by Nrl promoter and temporal expression profiling of flow-sorted photoreceptors. *Proc Natl Acad Sci U S A, 103*(10), 3890-3895. doi:10.1073/pnas.0508214103

Altimus, C. M., Guler, A. D., Alam, N. M., Arman, A. C., Prusky, G. T., Sampath, A. P., & Hattar, S. (2010). Rod photoreceptors drive circadian photoentrainment across a wide range of light intensities. *Nat Neurosci, 13*(9), 1107-1112. doi:10.1038/nn.2617

Applebury, M. L., Antoch, M. P., Baxter, L. C., Chun, L. L., Falk, J. D., Farhangfar, F., . . . Robbins, J. T. (2000). The murine cone photoreceptor: a single cone type expresses both S and M opsins with retinal spatial patterning. *Neuron, 27*(3), 513-523. doi:10.1016/s0896-6273(00)00062-3

Baba, K., Piano, I., Lyuboslavsky, P., Chrenek, M. A., Sellers, J. T., Zhang, S., . . . Iuvone, P. M. (2018). Removal of clock gene Bmal1 from the retina affects retinal development and accelerates cone photoreceptor degeneration during aging. *Proc Natl Acad Sci U S A, 115*(51), 13099-13104. doi:10.1073/pnas.1808137115

Bobu, C., Sandu, C., Laurent, V., Felder-Schmittbuhl, M. P., & Hicks, D. (2013). Prolonged light exposure induces widespread phase shifting in the circadian clock and visual pigment gene expression of the Arvicanthis ansorgei retina. *Mol Vis, 19*, 1060-1073.

Boudard, D. L., Mendoza, J., & Hicks, D. (2009). Loss of photic entrainment at low illuminances in rats with acute photoreceptor degeneration. *Eur J Neurosci, 30*(8), 1527-1536. doi:EJN6935 [pii]
10.1111/j.1460-9568.2009.06935.x

Butler, M. P., & Silver, R. (2011). Divergent photic thresholds in the non-image-forming visual system: entrainment, masking and pupillary light reflex. *Proc Biol Sci, 278*(1706), 745-750. doi:10.1098/rspb.2010.1509

Calligaro, H., Coutanson, C., Najjar, R. P., Mazzaro, N., Cooper, H. M., Haddjeri, N., . . . Dkhissi-Benyahya, O. (2019). Rods contribute to the light-induced phase shift of the retinal clock in mammals. *PLoS Biol, 17*(3), e2006211. doi:10.1371/journal.pbio.2006211

Daniele, L. L., Lillo, C., Lyubarsky, A. L., Nikonov, S. S., Philp, N., Mears, A. J., . . . Pugh, E. N., Jr. (2005). Cone-like morphological, molecular, and electrophysiological features of the photoreceptors of the Nrl knockout mouse. *Invest Ophthalmol Vis Sci, 46*(6), 2156-2167. doi:10.1167/iovs.04-1427

Dkhissi-Benyahya, O., Coutanson, C., Knoblauch, K., Lahouaoui, H., Leviel, V., Rey, C., . . . Cooper, H. M. (2013). The absence of melanopsin alters retinal clock function and dopamine regulation by light. *Cell Mol Life Sci, 70*(18), 3435-3447. doi:10.1007/s00018-013-1338-9

Dkhissi-Benyahya, O., Gronfier, C., De Vanssay, W., Flamant, F., & Cooper, H. M. (2007). Modeling the role of mid-wavelength cones in circadian responses to light. *Neuron, 53*(5), 677-687. doi:S0896-6273(07)00104-3 [pii]
10.1016/j.neuron.2007.02.005

Edgar, D. M., Martin, C. E., & Dement, W. C. (1991). Activity feedback to the mammalian circadian pacemaker: influence on observed measures of rhythm period length. *J Biol Rhythms, 6*(3), 185-199. doi:10.1177/074873049100600301

Felder-Schmittbuhl, M. P., Buhr, E. D., Dkhissi-Benyahya, O., Hicks, D., Peirson, S. N., Ribelayga, C. P., . . . Tosini, G. (2018). Ocular Clocks: Adapting Mechanisms for Eye Functions and Health. *Invest Ophthalmol Vis Sci, 59*(12), 4856-4870. doi:10.1167/iovs.18-24957

Felder-Schmittbuhl, M. P., Calligaro, H., & Dkhissi-Benyahya, O. (2017). The retinal clock in mammals: role in health and disease. *Chronophysiology Ther., 7*, 33-45. doi:doi:10.2147/CPT.S115251

Gianesini, C., Clesse, D., Tosini, G., Hicks, D., & Laurent, V. (2015). Unique Regulation of the Melatonin Synthetic Pathway in the Retina of Diurnal Female Arvicanthis ansorgei (Rodentia). *Endocrinology, 156*(9), 3292-3308. doi:10.1210/EN.2015-1267

Goz, D., Studholme, K., Lappi, D. A., Rollag, M. D., Provencio, I., & Morin, L. P. (2008). Targeted destruction of photosensitive retinal ganglion cells with a saporin conjugate alters the effects of light on mouse circadian rhythms. *PLoS One, 3*(9), e3153. doi:10.1371/journal.pone.0003153

Guler, A. D., Ecker, J. L., Lall, G. S., Haq, S., Altimus, C. M., Liao, H. W., . . . Hattar, S. (2008). Melanopsin cells are the principal conduits for rod-cone input to non-image-forming vision. *Nature, 453*(7191), 102-105. doi:10.1038/nature06829

Haque, R., Ali, F. G., Biscoglia, R., Abey, J., Weller, J., Klein, D., & Iuvone, P. M. (2010). CLOCK and NPAS2 have overlapping roles in the circadian oscillation of arylalkylamine N-acetyltransferase mRNA in chicken cone photoreceptors. *J Neurochem, 113*(5), 1296-1306. doi:10.1111/j.1471-4159.2010.06698.x

Hastings, M. H., Maywood, E. S., & Brancaccio, M. (2019). The Mammalian Circadian Timing System and the Suprachiasmatic Nucleus as Its Pacemaker. *Biology (Basel), 8*(1). doi:10.3390/biology8010013

Hatori, M., Le, H., Vollmers, C., Keding, S. R., Tanaka, N., Buch, T., . . . Panda, S. (2008). Inducible ablation of melanopsin-expressing retinal ganglion cells reveals their central role in non-image forming visual responses. *PLoS One, 3*(6), e2451. doi:10.1371/journal.pone.0002451

Hellemans, J., Mortier, G., De Paepe, A., Speleman, F., & Vandesompele, J. (2007). qBase relative quantification framework and software for management and automated analysis of real-time quantitative PCR data. *Genome Biol, 8*(2), R19. doi:10.1186/gb-2007-8-2-r19

Hughes, S., Jagannath, A., Hankins, M. W., Foster, R. G., & Peirson, S. N. (2015). Photic regulation of clock systems. *Methods Enzymol, 552*, 125-143. doi:10.1016/bs.mie.2014.10.018

Hughes, S., Watson, T. S., Foster, R. G., Peirson, S. N., & Hankins, M. W. (2013). Nonuniform distribution and spectral tuning of photosensitive retinal ganglion cells of the mouse retina. *Curr Biol, 23*(17), 1696-1701. doi:10.1016/j.cub.2013.07.010

Jaeger, C., Sandu, C., Malan, A., Mellac, K., Hicks, D., & Felder-Schmittbuhl, M. P. (2015). Circadian organization of the rodent retina involves strongly coupled, layer-specific oscillators. *FASEB J, 29*(4), 1493-1504. doi:10.1096/fj.14-261214

Jeon, C. J., Strettoi, E., & Masland, R. H. (1998). The major cell populations of the mouse retina. *J Neurosci, 18*(21), 8936-8946.

King, D. P., & Takahashi, J. S. (2000). Molecular genetics of circadian rhythms in mammals. *Annu Rev Neurosci, 23*, 713-742. doi:10.1146/annurev.neuro.23.1.713

Klarsfeld, A., Leloup, J. C., & Rouyer, F. (2003). Circadian rhythms of locomotor activity in Drosophila. *Behav Processes, 64*(2), 161-175. doi:10.1016/s0376-6357(03)00133-5

Krigel, A., Felder-Schmittbuhl, M. P., & Hicks, D. (2010). Circadian-clock driven cone-like photoreceptor phagocytosis in the neural retina leucine zipper gene knockout mouse. *Mol Vis, 16*, 2873-2881. doi:308 [pii]

Lall, G. S., Revell, V. L., Momiji, H., Al Enezi, J., Altimus, C. M., Guler, A. D., . . . Lucas, R. J. (2010). Distinct contributions of rod, cone, and melanopsin photoreceptors to encoding irradiance. *Neuron, 66*(3), 417-428. doi:10.1016/j.neuron.2010.04.037

Laranjeiro, R., & Whitmore, D. (2014). Transcription factors involved in retinogenesis are co-opted by the circadian clock following photoreceptor differentiation. *Development, 141*(13), 2644-2656. doi:10.1242/dev.104380

Li, P., Chaurasia, S. S., Gao, Y., Carr, A. L., Iuvone, P. M., & Li, L. (2008). CLOCK is required for maintaining the circadian rhythms of Opsin mRNA expression in photoreceptor cells. *J Biol Chem, 283*(46), 31673-31678. doi:10.1074/jbc.M803875200

Li, W., & DeVries, S. H. (2004). Separate blue and green cone networks in the mammalian retina. *Nat Neurosci, 7*(7), 751-756. doi:10.1038/nn1275

Liu, X., Zhang, Z., & Ribelayga, C. P. (2012). Heterogeneous expression of the core circadian clock proteins among neuronal cell types in mouse retina. *PLoS One, 7*(11), e50602. doi:10.1371/journal.pone.0050602

McMahon, D. G., Iuvone, P. M., & Tosini, G. (2014). Circadian organization of the mammalian retina: from gene regulation to physiology and diseases. *Prog Retin Eye Res, 39*, 58-76. doi:10.1016/j.preteyeres.2013.12.001

Mears, A. J., Kondo, M., Swain, P. K., Takada, Y., Bush, R. A., Saunders, T. L., . . . Swaroop, A. (2001). Nrl is required for rod photoreceptor development. *Nat Genet, 29*(4), 447-452. doi:10.1038/ng774

Mendoza, J., Graff, C., Dardente, H., Pevet, P., & Challet, E. (2005). Feeding cues alter clock gene oscillations and photic responses in the suprachiasmatic nuclei of mice exposed to a light/dark cycle. *J Neurosci, 25*(6), 1514-1522. doi:10.1523/JNEUROSCI.4397-04.2005

Mouland, J. W., Martial, F., Watson, A., Lucas, R. J., & Brown, T. M. (2019). Cones Support Alignment to an Inconsistent World by Suppressing Mouse Circadian Responses to the Blue Colors Associated with Twilight. *Curr Biol, 29*(24), 4260-4267 e4264. doi:10.1016/j.cub.2019.10.028

Mrosovsky, N. (2003). Contribution of classic photoreceptors to entrainment. *J Comp Physiol A Neuroethol Sens Neural Behav Physiol, 189*(1), 69-73. doi:10.1007/s00359-002-0378-7

Mrosovsky, N., Foster, R. G., & Salmon, P. A. (1999). Thresholds for masking responses to light in three strains of retinally degenerate mice. *J Comp Physiol A, 184*(4), 423-428. doi:10.1007/s003590050341

Mrosovsky, N., & Hattar, S. (2003). Impaired masking responses to light in melanopsin-knockout mice. *Chronobiol Int, 20*(6), 989-999. doi:10.1081/cbi-120026043

Munteanu, T., Noronha, K. J., Leung, A. C., Pan, S., Lucas, J. A., & Schmidt, T. M. (2018). Light-dependent pathways for dopaminergic amacrine cell development and function. *Elife, 7*. doi:10.7554/eLife.39866

Nelson, W., Tong, Y. L., Lee, J. K., & Halberg, F. (1979). Methods for cosinor-rhythmometry. *Chronobiologia, 6*(4), 305-323.

Niki, T., Hamada, T., Ohtomi, M., Sakamoto, K., Suzuki, S., Kako, K., . . . Ishida, N. (1998). The localization of the site of arylalkylamine N-acetyltransferase circadian expression in the photoreceptor cells of mammalian retina. *Biochem Biophys Res Commun, 248*(1), 115-120. doi:10.1006/bbrc.1998.8916

Nikonov, S. S., Daniele, L. L., Zhu, X., Craft, C. M., Swaroop, A., & Pugh, E. N., Jr. (2005). Photoreceptors of Nrl -/- mice coexpress functional S- and M-cone opsins having distinct inactivation mechanisms. *J Gen Physiol, 125*(3), 287-304. doi:10.1085/jgp.200409208

Nir, I., & Iuvone, P. M. (1994). Alterations in light-evoked dopamine metabolism in dystrophic retinas of mutant rds mice. *Brain Res, 649*(1-2), 85-94. doi:10.1016/0006-8993(94)91051-0

Noguchi, T., Michihata, T., Nakamura, W., Takumi, T., Shimizu, R., Yamamoto, M., . . . Nakajima, Y. (2010). Dual-color luciferase mouse directly demonstrates coupled expression of two clock genes. *Biochemistry, 49*(37), 8053-8061. doi:10.1021/bi100545h

Oishi, K., Sakamoto, K., Okada, T., Nagase, T., & Ishida, N. (1998). Antiphase circadian expression between BMAL1 and period homologue mRNA in the suprachiasmatic nucleus and peripheral tissues of rats. *Biochem Biophys Res Commun, 253*(2), 199-203. doi:10.1006/bbrc.1998.9779

Pendergast, J. S., Friday, R. C., & Yamazaki, S. (2010). Photic entrainment of period mutant mice is predicted from their phase response curves. *J Neurosci, 30*(36), 12179-12184. doi:10.1523/JNEUROSCI.2607-10.2010

Perez-Fernandez, V., Milosavljevic, N., Allen, A. E., Vessey, K. A., Jobling, A. I., Fletcher, E. L., . . . Cameron, M. A. (2019). Rod Photoreceptor Activation Alone Defines the Release of Dopamine in the Retina. *Curr Biol, 29*(5), 763-774 e765. doi:10.1016/j.cub.2019.01.042

Pierce, M. E., Sheshberadaran, H., Zhang, Z., Fox, L. E., Applebury, M. L., & Takahashi, J. S. (1993). Circadian regulation of iodopsin gene expression in embryonic photoreceptors in retinal cell culture. *Neuron, 10*(4), 579-584. doi:10.1016/0896-6273(93)90161-j

Provencio, I., & Foster, R. G. (1995). Circadian rhythms in mice can be regulated by photoreceptors with cone-like characteristics. *Brain Res, 694*(1-2), 183-190. doi:10.1016/0006-8993(95)00694-l

Provencio, I., Rollag, M. D., & Castrucci, A. M. (2002). Photoreceptive net in the mammalian retina. This mesh of cells may explain how some blind mice can still tell day from night. *Nature, 415*(6871), 493. doi:10.1038/415493a

Roger, J. E., Ranganath, K., Zhao, L., Cojocaru, R. I., Brooks, M., Gotoh, N., . . . Swaroop, A. (2012). Preservation of cone photoreceptors after a rapid yet transient degeneration and remodeling in cone-only Nrl-/- mouse retina. *J Neurosci, 32*(2), 528-541. doi:10.1523/JNEUROSCI.3591-11.2012

Ruan, G. X., Allen, G. C., Yamazaki, S., & McMahon, D. G. (2008). An autonomous circadian clock in the inner mouse retina regulated by dopamine and GABA. *PLoS Biol, 6*(10), e249. doi:10.1371/journal.pbio.0060249

Ruan, G. X., Zhang, D. Q., Zhou, T., Yamazaki, S., & McMahon, D. G. (2006). Circadian organization of the mammalian retina. *Proc Natl Acad Sci U S A, 103*(25), 9703-9708. doi:10.1073/pnas.0601940103

Sakamoto, K., Liu, C., Kasamatsu, M., Iuvone, P. M., & Tosini, G. (2006). Intraocular injection of kainic acid does not abolish the circadian rhythm of arylalkylamine N-acetyltransferase mRNA in rat photoreceptors. *Mol Vis, 12*, 117-124.

Sakamoto, K., Liu, C., & Tosini, G. (2004). Classical photoreceptors regulate melanopsin mRNA levels in the rat retina. *J Neurosci, 24*(43), 9693-9697. doi:24/43/9693 [pii]
10.1523/JNEUROSCI.2556-04.2004

Salaberry, N. L., Hamm, H., Felder-Schmittbuhl, M. P., & Mendoza, J. (2019). A suprachiasmatic-independent circadian clock(s) in the habenula is affected by Per gene mutations and housing light conditions in mice. *Brain Struct Funct, 224*(1), 19-31. doi:10.1007/s00429-018-1756-4

Sandu, C., Hicks, D., & Felder-Schmittbuhl, M. P. (2011). Rat photoreceptor circadian oscillator strongly relies on lighting conditions. *Eur J Neurosci, 34*(3), 507-516. doi:10.1111/j.1460-9568.2011.07772.x

Spoelstra, K., & Daan, S. (2008). Effects of constant light on circadian rhythmicity in mice lacking functional cry genes: dissimilar from per mutants. *J Comp Physiol A Neuroethol Sens Neural Behav Physiol, 194*(3), 235-242. doi:10.1007/s00359-007-0301-3

Steinlechner, S., Jacobmeier, B., Scherbarth, F., Dernbach, H., Kruse, F., & Albrecht, U. (2002). Robust circadian rhythmicity of Per1 and Per2 mutant mice in constant light, and dynamics of Per1 and Per2 gene expression under long and short photoperiods. *J Biol Rhythms, 17*(3), 202-209. doi:10.1177/074873040201700303

Storch, K. F., Paz, C., Signorovitch, J., Raviola, E., Pawlyk, B., Li, T., & Weitz, C. J. (2007). Intrinsic circadian clock of the mammalian retina: importance for retinal processing of visual information. *Cell, 130*(4), 730-741. doi:10.1016/j.cell.2007.06.045

Szel, A., & Rohlich, P. (1992). Two cone types of rat retina detected by anti-visual pigment antibodies. *Exp Eye Res, 55*(1), 47-52. doi:10.1016/0014-4835(92)90090-f

Takahashi, J. S. (2017). Transcriptional architecture of the mammalian circadian clock. *Nat Rev Genet, 18*(3), 164-179. doi:10.1038/nrg.2016.150

Thompson, S., Foster, R. G., Stone, E. M., Sheffield, V. C., & Mrosovsky, N. (2008). Classical and melanopsin photoreception in irradiance detection: negative masking of locomotor activity by light. *Eur J Neurosci, 27*(8), 1973-1979. doi:10.1111/j.1460-9568.2008.06168.x

Thompson, S., Recober, A., Vogel, T. W., Kuburas, A., Owens, J. A., Sheffield, V. C., . . . Stone, E. M. (2010). Light aversion in mice depends on nonimage-forming irradiance detection. *Behav Neurosci, 124*(6), 821-827. doi:10.1037/a0021568

Thompson, S., Stasheff, S. F., Hernandez, J., Nylen, E., East, J. S., Kardon, R. H., . . . Stone, E. M. (2011). Different inner retinal pathways mediate rod-cone input in irradiance detection for the pupillary light reflex and regulation of behavioral state in mice. *Invest Ophthalmol Vis Sci, 52*(1), 618-623. doi:10.1167/iovs.10-6146

Tosini, G., Davidson, A. J., Fukuhara, C., Kasamatsu, M., & Castanon-Cervantes, O. (2007). Localization of a circadian clock in mammalian photoreceptors. *FASEB J, 21*(14), 3866-3871. doi:10.1096/fj.07-8371com

Tosini, G., & Menaker, M. (1996). Circadian rhythms in cultured mammalian retina. *Science, 272*(5260), 419-421.

van Diepen, H. C., Ramkisoensing, A., Peirson, S. N., Foster, R. G., & Meijer, J. H. (2013). Irradiance encoding in the suprachiasmatic nuclei by rod and cone photoreceptors. *FASEB J, 27*(10), 4204-4212. doi:10.1096/fj.13-233098

van Oosterhout, F., Fisher, S. P., van Diepen, H. C., Watson, T. S., Houben, T., VanderLeest, H. T., . . . Meijer, J. H. (2012). Ultraviolet light provides a major input to non-image-forming light detection in mice. *Curr Biol, 22*(15), 1397-1402. doi:10.1016/j.cub.2012.05.032

von Schantz, M., Lucas, R. J., & Foster, R. G. (1999). Circadian oscillation of photopigment transcript levels in the mouse retina. *Brain Res Mol Brain Res, 72*(1), 108-114. doi:S0169328X99002090 [pii]

Walmsley, L., Hanna, L., Mouland, J., Martial, F., West, A., Smedley, A. R., . . . Brown, T. M. (2015). Colour as a signal for entraining the mammalian circadian clock. *PLoS Biol, 13*(4), e1002127. doi:10.1371/journal.pbio.1002127

PBIOLOGY-D-14-03915 [pii]

Welsh, D. K., Takahashi, J. S., & Kay, S. A. (2010). Suprachiasmatic nucleus: cell autonomy and network properties. *Annu Rev Physiol, 72*, 551-577. doi:10.1146/annurev-physiol-021909-135919

Wenzel, A., von Lintig, J., Oberhauser, V., Tanimoto, N., Grimm, C., & Seeliger, M. W. (2007). RPE65 is essential for the function of cone photoreceptors in NRL-deficient mice. *Invest Ophthalmol Vis Sci, 48*(2), 534-542. doi:10.1167/iovs.06-0652

Yamazaki, S., Goto, M., & Menaker, M. (1999). No evidence for extraocular photoreceptors in the circadian system of the Syrian hamster. *J Biol Rhythms, 14*(3), 197-201. doi:10.1177/074873099129000605

Yoo, S. H., Yamazaki, S., Lowrey, P. L., Shimomura, K., Ko, C. H., Buhr, E. D., . . . Takahashi, J. S. (2004). PERIOD2::LUCIFERASE real-time reporting of circadian dynamics reveals persistent circadian oscillations in mouse peripheral tissues. *Proc Natl Acad Sci U S A, 101*(15), 5339-5346. doi:10.1073/pnas.0308709101